5-1-1989

Theory and Simulation of the Brushless DC 120° Inverter System

Scott D. Sudhoff
Purdue University

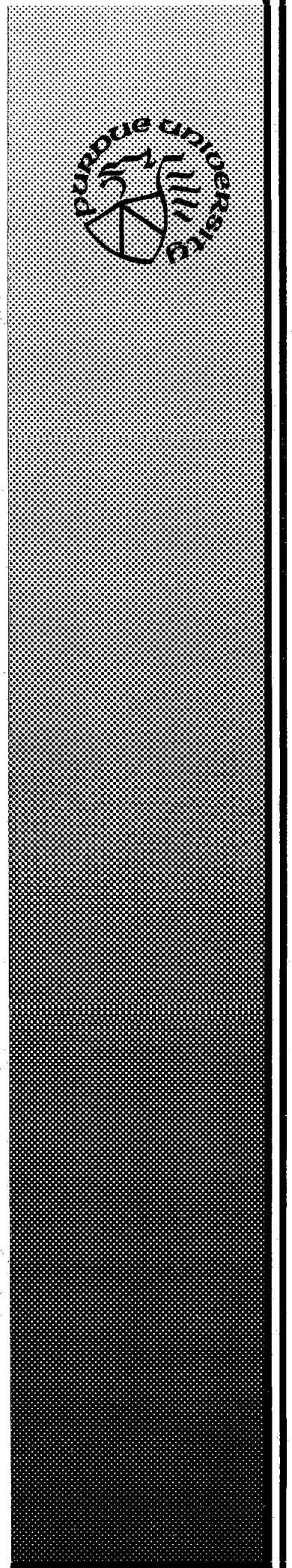

Theory and Simulation of the Brushless DC 120° Inverter System

S. D. Sudhoff

TR-EE 89-25
May, 1989

School of Electrical Engineering
Purdue University
West Lafayette, Indiana 47907

THEORY AND SIMULATION OF THE BRUSHLESS DC 120° INVERTER SYSTEM

A Thesis

Submitted to the Faculty

of

Purdue University

by

Scott D. Sudhoff

In Partial Fulfillment of the

Requirements for the Degree

of

Master of Science in Electrical Engineering

May 1989

this is dedicated
to my parents and
to my wife Julie

ACKNOWLEDGMENTS

I thank Professor Paul Krause for his enthusiasm and guidance over the past year. I also thank Lisa Reeves, Wanda Booth, and Linda Stovall for help in the preparation of this thesis.

TABLE OF CONTENTS

Page

LIST OF TABLES vi

LIST OF FIGURES vii

ABSTRACT ix

CHAPTER 1 - INTRODUCTION 1

CHAPTER 2 - DESCRIPTION OF THE BRUSHLESS DC MACHINE 3

Machine Equations 3
Machine Equations in the Rotor Reference Frame 5

CHAPTER 3 - INVERTER OPERATION 8

Basic Operation 8
The 180° Inverter 10
The 120° Inverter 11

CHAPTER 4 - ANALYSIS OF STEADY STATE PERFORMANCE 19

Symmetry of Inverter Operation 19
Current Waveforms For Constant Speed Operation 22

Page

CHAPTER 5 - SIMULATION OF STEADY STATE PERFORMANCE 26

The Algorithm 26
Computing Block Diagram 27
Average Torque Calculations 32

CHAPTER 6 - OPERATIONAL MODES 35

Classification Scheme 35
Typical Behavior 37
Inverter Behavior vs Frequency 45

CHAPTER 7 - ANALYTICAL APPROXIMATIONS 50

Approximation A 50
Approximation B 50
Approximation C 52
Comparison of Methods 52

CHAPTER 8 - CONCLUSION 57

LIST OF REFERENCES 58

APPENDIX 59

LIST OF TABLES

Table Page

3.1 180° Inverter Operation 11

3.2 120° Inverter Operation 12

3.3 BSI II Operation 13

6.1 Waveform Data 37

7.1 120° Inverter Operation with Resistive Load 51

7.2 Comparison of Approximations 53

A.1 Machine Parameters 59

LIST OF FIGURES

Figure — Page

2.1 Permanent Magnet Synchronous Machine 4

3.1 Inverter and Machine 9

3.2 Intervals in BSI II - Example 1 15

3.3 Graphical Depiction of Domains 17

3.4 Intervals in BSI II - Example 2 18

4.1 Equivalent Circuit During BSI I 20

4.2 Equivalent Circuit During BSI II 20

4.3 Same as Fig 4.2 with Polarity and Directions Reversed 21

4.4 Fig 4.3, Rearranged 21

5.1 Computing Block Diagram 28

6.1 Modes on the ω_r - ϕ Plane 36

6.2 The NZ Mode 38

6.3 The NPZ Mode 40

6.4 The N Mode 41

6.5 The NZN Mode 42

Figure Page

6.6 The NP Mode 43

6.7 The PZ Mode 44

6.8 Interval Map for $\phi = 0°$ 46

6.9 Interval Map for $\phi = 30°$ 47

6.10 Interval Map for $\phi = 60°$ 48

6.11 Interval Map for $\phi = 90°$ 49

7.1 Torque Comparison for $\phi = 0°$ 54

7.2 Torque Comparison for $\phi = 30°$ 55

7.3 Torque Comparison for $\phi = 60°$ 56

ABSTRACT

Sudhoff, Scott D., M.S.E.E., Purdue University, May 1989. Theory and Simulation of the Brushless DC 120° Inverter System. Major Professor: Paul C Krause.

The brushless dc motor- inverter system is becoming increasingly popular in servo and variable speed applications. One type of inverter, the 120° inverter, does not require rotor position sensing hardware. In this thesis, a theory of the brushless dc motor with a 120° inverter is set forth and used to create a fast simulation procedure for steady state operation. This simulation is well suited for evaluation of torque speed curves since the effects of changes of system parameters can be rapidly assessed. Furthermore, it was found that the system operation may be classified into a finite number of distinct operating modes. The properties of these modes and physical reason for their existence is discussed. Classifing the operation into modes provides a powerful tool for understanding system behavior. The theory presented and classification scheme are then used to formulate an approximate analytical method for the steady-state torque, which is quite accurate for normal operating conditions. The approximations presented are suitable for control system design.

CHAPTER 1
INTRODUCTION

The brushless dc motor is becoming a popular device for servo systems and variable speed applications. The machine itself is actually a permanent magnet synchronous machine. Its torque speed characteristics resemble those of a dc machine when the frequency of the applied voltages is made to correspond to the rotor speed. To achieve this, it is necessary to determine the rotor position which, in turn, is used to make up the applied voltages. There are several methods of accomplishing this. One common method of doing this is to measure the position of the rotor using Hall effect devices and then apply the necessary voltages using a 180° inverter. Another method is to use an optical encoder and a power amplifier. A third method is to use a 120° inverter, which differs from other schemes in that it is possible to determine the position of the rotor from the line to ground voltages of the machine. However, this particular inverter is difficult to analyize.

Recently, a method of simulating the brushless dc 120° inverter system was developed [1][2]. Unfortunately, some aspects of 120° inverter operation were not included in that analysis. It is the purpose of this thesis to set forth the complete operating theory of the brushless dc 120° inverter system.

In this thesis a description of the permanent magnet synchronous machine is set forth in chapter two. Next, 180° inverter operation is explained. The operation of the 180° inverter is then used as a basis for the explanation of the operation of the 120° inverter. This explanation is completed by defining the various phenomenon associated with 120° inverter operation in terms of the physical operation of the system.

The first step in the analysis of the machine inverter system is to make use of the symmetry of the system. It is then shown that, except for a finite number of discontinuities, the differential equations which govern the system are linear and easily solved. These two facts are brought together in the development of a computationally efficient method of simulation for steady state operation.

Next, it is shown that the brushless dc 120° inverter system operation can be classified into distinct operating modes. The characteristics of different modes and conditions which favor existence of these modes is discussed. As it turns out, the simulation method is extremely useful in exploring the different operating modes since mode recognition is inherent in the simulation.

In the final chapter, analytical techniques for estimating the torque speed characteristics of this device are presented. One of these approximations makes use of the mode classification techniques established earlier. It is found that this approximation accurately predicts the most common operating conditions.

CHAPTER 2
DESCRIPTION OF THE BRUSHLESS DC MACHINE

The term "brushless dc" is somewhat of a misnomer since the brushless dc machine is actually a permanent magnet synchronous motor such as the one depicted in Fig. 2.1. In fact, the only difference between the common notion of a permanent magnet synchronous machine and the brushless dc machine is in the form of the applied voltages. The reason the brushless dc machine is named as such is the similarity of its torque speed characteristics to those of an armature controlled dc machine.

In this chapter a background on the brushless dc machine is provided beginning with a description of the permanent magnet synchronous machine in machine variables. The machine equations are then transformed into the rotor reference frame. Finally, in the context of the rotor reference frame, the form of the applied voltages is specified. Additional background is given in [5] and [6].

Machine Equations

The purpose of this section is to establish the basic machine equations of the permanent magnet synchronous machine. The equations presented here are subject to the following assumptions: (1) the machine is non-salient, (2) the back emf is sinusoidal, and (3) the machine is wye connected. The voltage equation describing the brushless dc machine is given by (2.1) and the flux equation is given by (2.2).

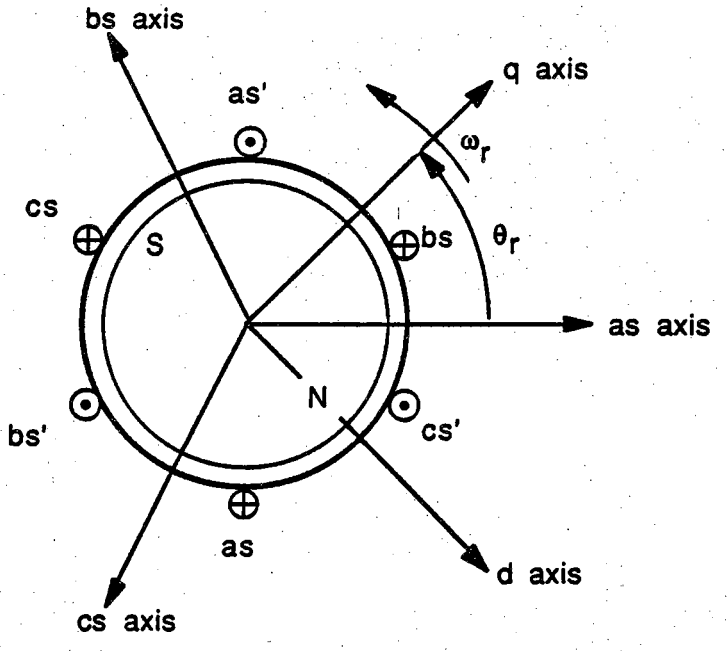

Figure 2.1 Permanent Magnet
Synchronous Machine

$$\vec{v}_{abcs} = r_s \vec{i}_{abcs} + \rho \vec{\lambda}_{abcs} \tag{2.1}$$

$$\vec{\lambda}_{abcs} = \begin{bmatrix} L & -M & -M \\ -M & L & -M \\ -M & -M & L \end{bmatrix} \vec{i}_{abcs} + \lambda'_m \begin{bmatrix} \sin\left(\Theta_r\right) \\ \sin\left(\Theta_r - \frac{2\pi}{3}\right) \\ \sin\left(\Theta_r + \frac{2\pi}{3}\right) \end{bmatrix} \tag{2.2}$$

Since the machine is wye connected, (2.2) may be rewritten as (2.3) where L_s is defined by (2.4). This representation is convenient since the three stator equations become uncoupled.

$$\vec{\lambda}_{abcs} = L_s \vec{i}_{abcs} + \lambda'_m \begin{bmatrix} \sin\left(\Theta_r\right) \\ \sin\left(\Theta_r - \frac{2\pi}{3}\right) \\ \sin\left(\Theta_r + \frac{2\pi}{3}\right) \end{bmatrix} \tag{2.3}$$

$$L_s = L + M \tag{2.4}$$

The instantaneous torque produced is

$$T_e = \left(\frac{P}{2}\right)\lambda'_m \left(\frac{3}{2} i_{as} \cos\left(\Theta_r\right) + \frac{\sqrt{3}}{2}\left(i_{bs} - i_{cs}\right)\sin\left(\Theta_r\right)\right) \tag{2.5}$$

Machine Equations in the Rotor Reference Frame

Considerable insight may be gained by making a change of variables which transforms all machine variables (abcs) to the rotor reference frame variables (qdos). The transformation from abcs variables to qd0s variables is given by (2.6) and (2.7) where $\vec{f}$ may stand for voltage, current, or flux linkage.

$$\vec{f}_{qd0s} = K_s^r \vec{f}_{abcs} \tag{2.6}$$

$$K_s^r = \frac{2}{3}\begin{bmatrix} \cos\left(\Theta_r\right) & \cos\left(\Theta_r - \frac{2\pi}{3}\right) & \cos\left(\Theta_r + \frac{2\pi}{3}\right) \\ \sin\left(\Theta_r\right) & \sin\left(\Theta_r - \frac{2\pi}{3}\right) & \sin\left(\Theta_r + \frac{2\pi}{3}\right) \\ \frac{1}{2} & \frac{1}{2} & \frac{1}{2} \end{bmatrix} \tag{2.7}$$

The inverse transformation is

$$\left(K_s^r\right)^{-1} = \begin{bmatrix} \cos\left(\Theta_r\right) & \sin\left(\Theta_r\right) & 1 \\ \cos\left(\Theta_r - \frac{2\pi}{3}\right) & \sin\left(\Theta_r - \frac{2\pi}{3}\right) & 1 \\ \cos\left(\Theta_r + \frac{2\pi}{3}\right) & \sin\left(\Theta_r + \frac{2\pi}{3}\right) & 1 \end{bmatrix} \tag{2.8}$$

Applying the transformation to the machine equations yields

$$v_{qs}^r = \left(r_s + \rho L_s\right) i_{qs}^r + \omega_r L_s i_{ds}^r + \omega_r \lambda_m' \tag{2.9}$$

$$v_{ds}^r = \left(r_s + \rho L_s\right) i_{ds}^r - \omega_r L_s i_{qs}^r \tag{2.10}$$

$$T_e = \left(\frac{3}{2}\right)\left(\frac{P}{2}\right)\lambda_m' i_{qs}^r \tag{2.11}$$

It can be seen from (2.11) that if torque is to be constant then i_{qs}^r must be constant. Hence, from (2.9) and (2.10), we see that for steady state operation v_{qs}^r and v_{ds}^r should be constant as well. Suppose

$$\vec{v}_{abcs} = \begin{bmatrix} V_s \cos\left(\theta_r + \alpha\right) \\ V_s \cos\left(\theta_r - \frac{2\pi}{3} + \alpha\right) \\ V_s \cos\left(\theta_r + \frac{2\pi}{3} + \alpha\right) \end{bmatrix} \tag{2.12}$$

Then, for any rotor speed, (2.13) and (2.14) apply. Note that if V_s is constant then so are v_{qs}^r and v_{ds}^r.

$$v_{qs}^r = V_s \cos\left(\alpha\right) \tag{2.13}$$

$$v_{ds}^r = -V_s \sin\left(\alpha\right) \tag{2.14}$$

For steady state conditions, with $\alpha = 0$ and $\omega_r L_s \ll r_s$, (2.13), (2.14), (2.9) - (2.11) may be manipulated to yield (2.15) which is identical in form to the steady state torque equation of an armature controlled dc machine.

$$T_e = \left(\frac{3}{2}\right)\left(\frac{P}{2}\right)\frac{\lambda_m'}{r_s}\left(V_s - \lambda_m' \omega_r\right) \tag{2.15}$$

Now that the basic features of brushless dc operation have been set forth, the problem of actually obtaining the voltages described by (2.12) will be addressed. One device used to obtain these voltages in practice is known as an inverter. The inverter is the subject of the next chapter.

CHAPTER 3
INVERTER OPERATION

There are several methods of achieving stator voltages of the form given by (2.12). One method is to sense the position of the rotor, look up the necessary instantaneous voltages in a table in ROM, and then produce the required voltages via a power amplifier as explained in [7]. While this method results in a high performance system, it is inefficient and thus has increased heat sink requirements.

A second method to achieve the required stator voltages is to use a device known as an inverter. Assuming ideal components the inverter operates without loss and thus has reduced transistor heat sink requirements. The tradeoff is that the voltages produced contain harmonics which increase loss in the stator circuits.

There are two types of inverters, the 120° and the 180°. In the 120° case, each transistor is on 120 out of 360 electrical degrees. Likewise, in the 180° case, each transistor is on 180 out of 360 electrical degrees. Although the 120° inverter is more difficult to handle analytically it has a practical advantage in that it can be operated without any rotor position sensors as described in [4].

Basic Operation

A symbolic depiction of the brushless dc inverter system appears in Fig 3.1. The inverter consists of six transistors, T1-T6, which are used to convert dc power to ac power and six diodes D1-D6 which are necessary to protect the transistors from the inductive nature of the load.

The first step toward the analyses of the inverter is to apply Kirchhoff's

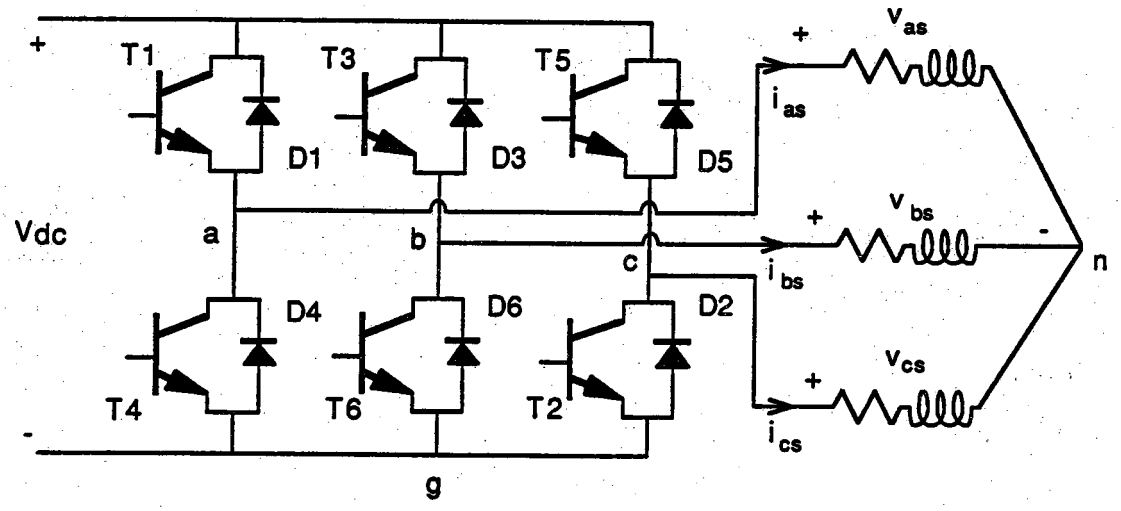

Figure 3.1 Inverter and Machine

voltage law to the three phases which yields

$$v_{ag} = v_{as} + v_{ng} \tag{3.1}$$

$$v_{bg} = v_{bs} + v_{ng} \tag{3.2}$$

$$v_{cg} = v_{cs} + v_{ng} \tag{3.3}$$

Kirchhoff's current law dictates

$$i_{as} + i_{bs} + i_{cs} = 0 \tag{3.4}$$

Equation (3.4) and (2.3) may be used to show that the sum of the stator flux linkages, namely $\lambda_{as} + \lambda_{bs} + \lambda_{cs}$, is zero. Since the sum of the stator currents is zero, and the sum of the stator flux linkages is zero, (2.1) tells us that

$$v_{as} + v_{bs} + v_{cs} = 0 \tag{3.5}$$

The neutral to ground voltage, v_{ng}, is obtained by adding (3.1), (3.2), and (3.3), and then subtracting (3.5) which results in

$$v_{ng} = \frac{1}{3}\left(v_{ag} + v_{bg} + v_{cg}\right) \tag{3.6}$$

Substituting (3.6) into (3.1), (3.2), and (3.3) yields

$$v_{as} = \frac{2}{3}v_{ag} - \frac{1}{3}v_{bg} - \frac{1}{3}v_{cg} \tag{3.7}$$

$$v_{bs} = \frac{2}{3}v_{bg} - \frac{1}{3}v_{ag} - \frac{1}{3}v_{cg} \tag{3.8}$$

$$v_{cs} = \frac{2}{3}v_{cg} - \frac{1}{3}v_{ag} - \frac{1}{3}v_{bg} \tag{3.9}$$

The 180° Inverter

The operation of the 180° inverter is set forth in Table 3.1. In the Table, electrical rotor position is divided into six 60° segments known as basic switching intervals (BSI). The second column specifies the center of each switching interval in terms of $\Theta_r - \phi$. The angle ϕ is known as the advance firing angle which allows the shifting of the transistor firing sequence relative to the position of the rotor. The third column of Table 3.1 defines the transistor firing sequence by indicating which transistors are gated on in a given BSI. The transistor firing pattern results in abcg and abcs voltages which are specified in Table 3.1.

Expressing the abcs voltages as given in Table 3.1 as a Fourier series in electrical rotor position, neglecting all harmonics, and incorporating the transformation to the rotor reference frame yields

Table 3.1 180° Inverter Operation

BSI	$\Theta_r - \phi$	Transistors On	v_{ag}	v_{bg}	v_{cg}	v_{as}	v_{bs}	v_{cs}
I	0°	1,2,6	V_{dc}	0	0	$\frac{2}{3} V_{dc}$	$-\frac{1}{3} V_{dc}$	$-\frac{1}{3} V_{dc}$
II	60°	1,2,3	V_{dc}	V_{dc}	0	$\frac{1}{3} V_{dc}$	$\frac{1}{3} V_{dc}$	$-\frac{2}{3} V_{dc}$
III	120°	2,3,4	0	V_{dc}	0	$-\frac{1}{3} V_{dc}$	$\frac{2}{3} V_{dc}$	$-\frac{1}{3} V_{dc}$
IV	180°	3,4,5	0	V_{dc}	V_{dc}	$-\frac{2}{3} V_{dc}$	$\frac{1}{3} V_{dc}$	$\frac{1}{3} V_{dc}$
V	240°	4,5,6	0	0	V_{dc}	$-\frac{1}{3} V_{dc}$	$-\frac{1}{3} V_{dc}$	$\frac{2}{3} V_{dc}$
VI	300°	1,5,6	V_{dc}	0	V_{dc}	$\frac{1}{3} V_{dc}$	$-\frac{2}{3} V_{dc}$	$\frac{1}{3} V_{dc}$

$$v_{qs}^r = \frac{2V_{dc}}{\pi} \cos\left(\phi\right) \tag{3.10}$$

$$v_{ds}^r = -\frac{2V_{dc}}{\pi} \sin\left(\phi\right) \tag{3.11}$$

Comparing (3.10) and (3.11) to (2.13) and (2.14) we see that for the 180° inverter α and ϕ are equivalent.

The 120° Inverter

The operation of a 120° inverter is summarized in Table 3.2, which is much the same as Table 3.1 except for two important differences. The first is that only two transistors are gated on at any given instant of time. Secondly, question marks appear periodically in the last three columns to indicate the fact that this voltage is determined by the instantaneous current in the corresponding phase.

The dependence of the phase voltages on the direction of current in the phase in which neither transistor is gated on is best illustrated by examining one specific BSI. In BSI II if $i_{bs} < 0$ then current will flow through D3 and thus $v_{bg} = V_{dc}$. Conversely, if $i_{bs} > 0$ then current flows through D6 which causes $v_{bg} = 0$. Finally, if $i_{bs} = 0$, then v_{bs} is the open circuit voltage as given by

$$v_{bs} = \lambda'_m \omega_r \cos\left(\Theta_r - \frac{2\pi}{3}\right) \tag{3.12}$$

If (3.2) is substituted into (3.6) we obtain

$$v_{ng} = \frac{1}{2}\left(v_{ag} + v_{bs} + v_{cg}\right) \tag{3.13}$$

for the neutral to ground voltage. Upon replacing v_{bs} with (3.12) in (3.13) and then using (3.13) to replace v_{ng} in (3.2) we arrive at

$$v_{bg} = \frac{1}{2}V_{dc} + \frac{3}{2}\lambda'_m \omega_r \cos\left(\Theta_r - \frac{2\pi}{3}\right) \tag{3.14}$$

Another application of (3.13) is to find v_{as} and v_{cs} from (3.1) and (3.3).

$$v_{as} = \frac{1}{2}V_{dc} - \frac{1}{2}\lambda'_m \omega_r \cos\left(\Theta_r - \frac{2\pi}{3}\right) \tag{3.15}$$

$$v_{cs} = -\frac{1}{2}V_{dc} - \frac{1}{2}\lambda'_m \omega_r \cos\left(\Theta_r - \frac{2\pi}{3}\right) \tag{3.16}$$

Table 3.3 summarizes the above paragraphs and identifies three different intervals which have not yet been explained. An N interval is segment of BSI

II for which $i_{bs} < 0$. Similarly, a P interval is a segment for which $i_{bs} > 0$. Finally, a Z interval occurs when $i_{bs} = 0$; however a zero crossing of i_{bs} is not considered a Z interval. The N, P, and Z intervals should not be confused with basic switching intervals (BSI).

Table 3.3 BSI II Operation

	Interval	v_{bg}	v_{as}	v_{bs}	v_{cs}
$i_{bs} < 0$	N	V_{dc}	$\frac{1}{3} V_{dc}$	$\frac{1}{3} V_{dc}$	$-\frac{2}{3} V_{dc}$
$i_{bs} > 0$	P	0	$\frac{2}{3} V_{dc}$	$-\frac{1}{3} V_{dc}$	$-\frac{1}{3} V_{dc}$
$i_{bs} = 0$	Z	(3.14)	(3.15)	(3.12)	(3.16)

Since the phase voltages are partially determined by the state of the phase current, a Fourier series cannot be written for the line to neutral voltages as was the case with the 180° inverter. This fact complicates the analysis; however, in exchange for this difficulty the back emf may be measured during Z intervals which eliminates the need for sensors [4].

In order to illustrate the N,P and Z intervals let us consider Fig. 3.2. Therein, i_{bs} and v_{bg} are plotted verses $\Theta_r - 30°$ over BSI II for $\omega_r = 150$ and $\phi = 0$. Initially, i_{bs} is negative. This N interval exists until i_{bs} goes to zero at which time a Z interval begins. The Z interval continues until a Z-N transition occurs, which results in an N interval that continues until the end of BSI II.

Transitions are defined to be the change from $i_{bs} = 0$ to either a N or P interval caused by the forward biasing of one of the diodes. Specifically, a Z-N transition occurs when v_{bg} would become greater than V_{dc} if i_{bs} remained at zero. This, of course, cannot occur since this causes diode D3 to become forward biased which limits v_{bg} at V_{dc} and causes i_{bs} to become negative. The second type of transition, a Z-P transition, occurs when v_{bg} would become negative if i_{bs} remained at zero. Again, this cannot occur because D6 becomes forward biased which causes v_{bg} to be limited at 0 and i_{bs} to become positive.

The domain of Θ_r over which Z-N and Z-P transitions will occur if $i_{bs} = 0$ can be calculated using (3.14). The Z-N domain is defined as the set of

Θ_r such that if $i_{bs} = 0$ a Z-N transition will occur. Using (3.14), we see that for a given rotor position Θ_r to be in the Z-N domain it must satisfy (3.17).

$$\cos\left(\Theta_r - \frac{2\pi}{3}\right) > \frac{V_{dc}}{3\lambda_m{}'\omega_r} \tag{3.17}$$

The Z-P domain is defined as the set of Θ_r such that if $i_{bs} = 0$ a Z-P transition will occur. A given rotor position Θ_r must satisfy (3.18) to be in the Z-P domain.

$$\cos\left(\Theta_r - \frac{2\pi}{3}\right) < -\frac{V_{dc}}{3\lambda_m{}'\omega_r} \tag{3.18}$$

Equation (3.17) and (3.18) have a graphical interpretation illustrated in Fig 3.3. Notice that as speed increases the Z-N and Z-P domains enlarge. Also notice that for $\omega_r < \frac{V_{dc}}{3\lambda_m{}'}$ the Z-N and Z-P domains are the empty set. Of primary interest is the portion of the Z-N and Z-P domains which lie within BSI II. For $\phi = 0$ only the Z-N domain intersects with BSI II. As ϕ increases, the Z-P domain intersects with the beginning portion of BSI II and the Z-N domain intersects with the concluding portion of BSI II. For $\phi = 90°$ we see that only the Z-P domain can intersect BSI II.

In addition to their relationship to Z-N and Z-P transitions, the Z-N and Z-P domains also have one other interesting property. Within a N (P) interval in the Z-N (Z-P) domain the current must remain negative (positive). Furthermore, within a N (P) interval outside the Z-N (Z-P) domain, the current will increase (decrease) towards zero. This is because the conditions which define the location of the domains ((3.17) and (3.18)) also determine the sign of the forcing function in the differential equation governing i_{bs} within the N and P intervals. This in turn implies that a N (P) interval cannot terminate within a Z-N (Z-P) domain unless the end of the switching interval is reached.

Another example of the definition of intervals and transitions is seen in Fig. 3.4. In Fig. 3.4, $\omega_r = 150$ Rad/S and $\phi = 60°$. As can be seen, operation begins with an N interval. At the point at which i_{bs} becomes zero, a Z-P

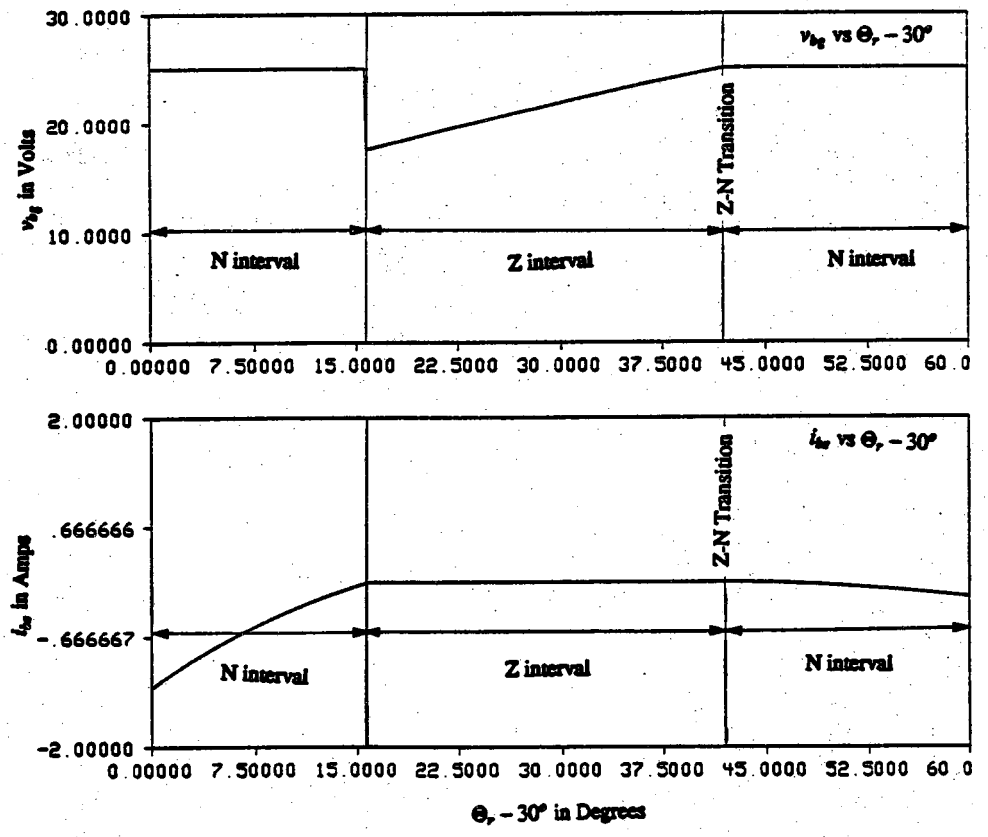

Figure 3.2 Intervals in BSI II - Example 1
$\omega_r = 150$ Rad/S $\phi = 0°$

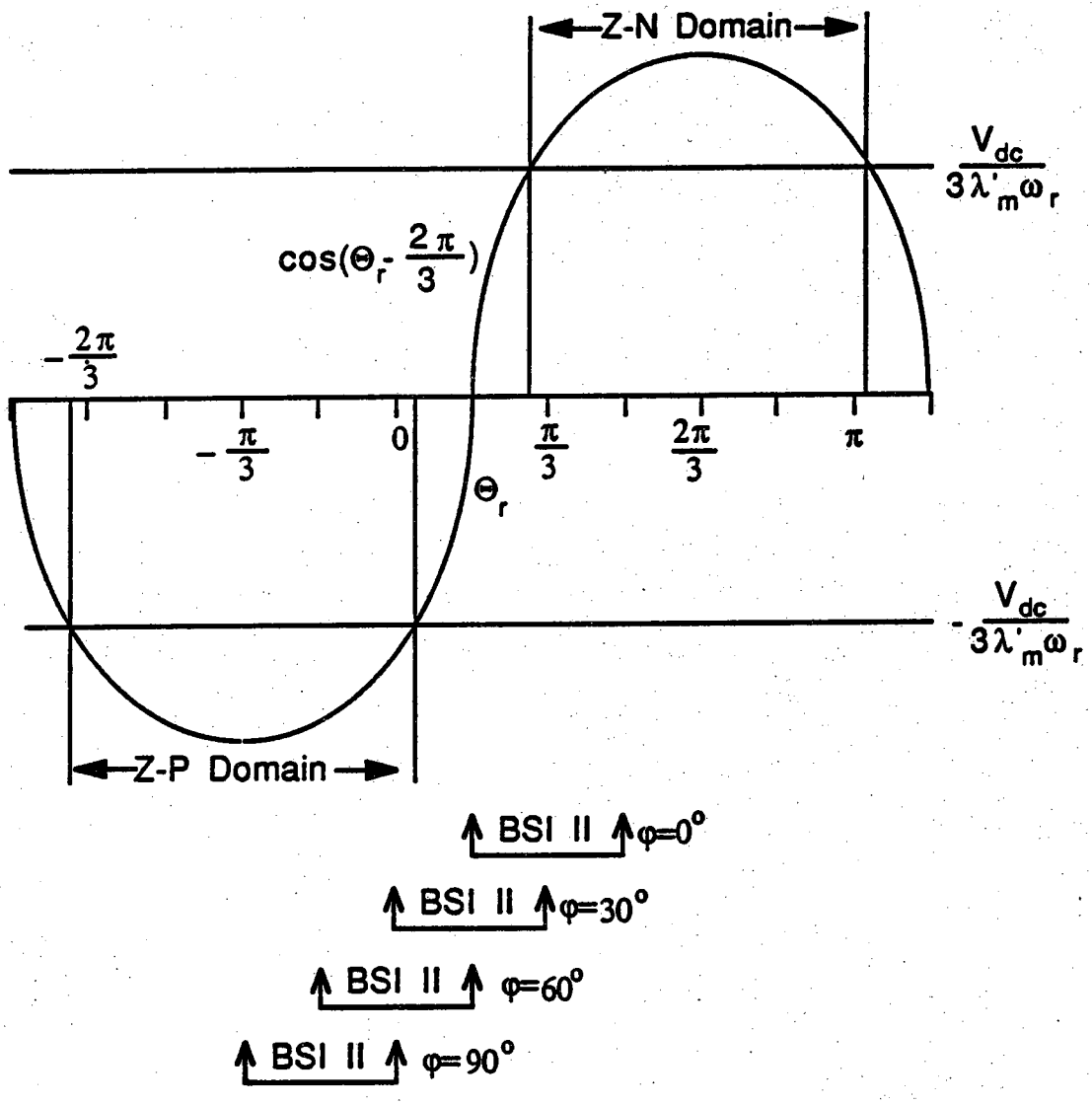

Figure 3.3 Graphical Depiction of Domains

transition occurs. After a Z-P transition occurs, i_{bs} cannot go to zero until Θ_r is no longer in the Z-P domain. Sometime after Θ_r has passes through the Z-P domain i_{bs} returns to zero thus marking the beginning of a Z period which lasts until the end of BSI II.

In the preceding paragraphs, the various phenomenon associated with inverter operation have been explained. In the next chapter, it will be shown that it is only necessary to consider BSI II when simulating steady state performance. Also, the differential equation associated with the N,P and Z intervals will be set forth and solved. Eventually, the result of this development will be an analytical/numerical simulation approach based on the intervals within BSI II.

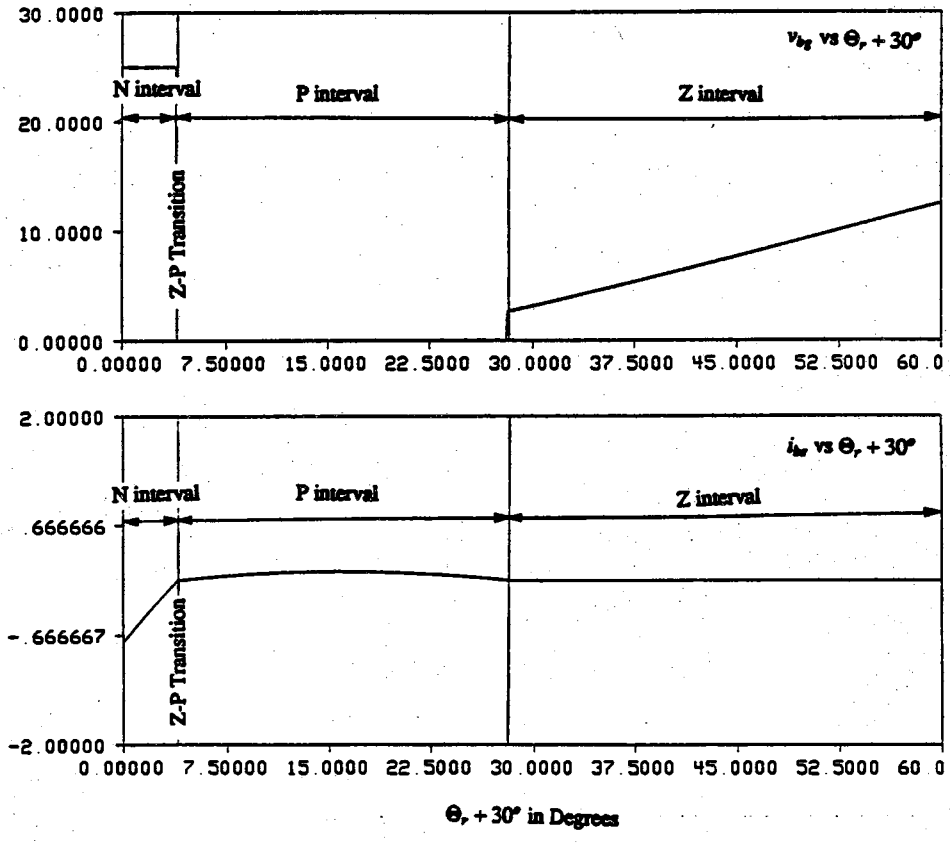

Figure 3.4 Intervals in BSI II - Example 2
$\omega_r = 150°$ and $\phi = 60°$

CHAPTER 4
ANALYSIS OF STEADY STATE PERFORMANCE

In [1], a method for determining the steady state waveforms of a brushless dc motor is described. As pointed out in [3] that work assumes that no Z-N or Z-P transitions occur, and that no P intervals exist. In this chapter, the work done in [1] is extended by removing these assumptions.

The development presented here has two parts. The first is to point out the symmetry conditions which exists between the BSI. Once the symmetry is established, the appropriate differential equations which describe each type of interval (N,P or Z) in BSI II are laid out and solved. This will set the stage for an analytical/numerical simulation.

Symmetry of Inverter Operation

It can be shown that the equivalent circuit during each switching interval is topologically related to the equivalent circuit during the previous interval. This relationship leads to a permuted equivalence of phase variables between BSI and to the symmetry of the waveforms.

Figure 4.1 shows the equivalent circuit during BSI I. In order to obtain the desired relationships, the equivalent circuit of BSI II will be shown to be identical to that of BSI I except for a permutation of the variables. The equivalent circuit for BSI II is shown in Fig. 4.2 where $\Theta_r^* = \Theta_r + 60^\circ$.

If one reverses the polarity of all voltages and the direction of all currents the equations which describe this circuit remain unchanged. This has been done in Fig. 4.3. Note that the diodes must be reversed in this manipulation. The next step is to rearrange the circuit as in Fig. 4.4.

Comparing Fig. 4.4 to Fig. 4.1 we see that in BSI II the as, bs, and cs variables are equivalent to the negative of the respective bs, as, and cs variables of BSI I. An identical relationship holds for all other adjacent pairs of switching intervals. For steady state conditions, the relationship between

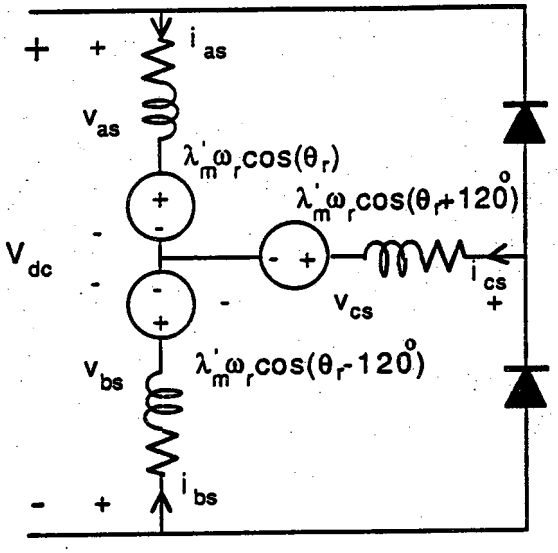

Figure 4.1 Equivalent Circuit During BSI I
$-30^{\circ} - \phi \leq \Theta_r \leq 30^{\circ} + \phi$

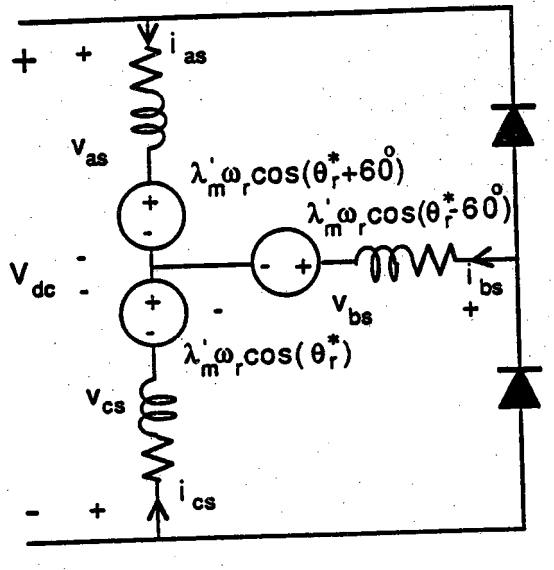

Figure 4.2 Equivalent Circuit During BSI II
$-30^{\circ} - \phi \leq \Theta^{*}_{r} \leq 30^{\circ} + \phi$

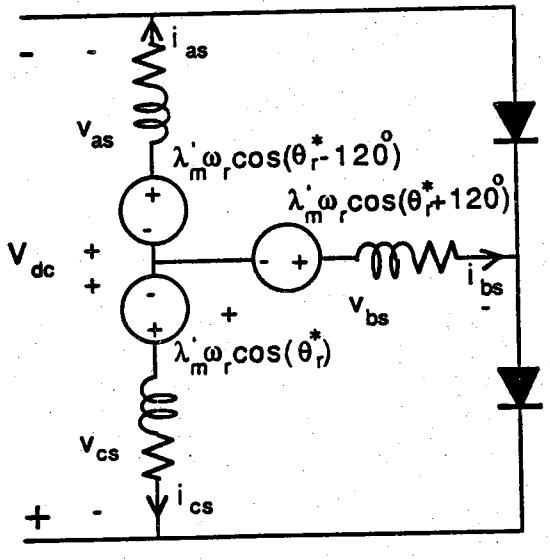

Figure 4.3 Same as Fig. 4.2 with
Polarity and Directions Reversed

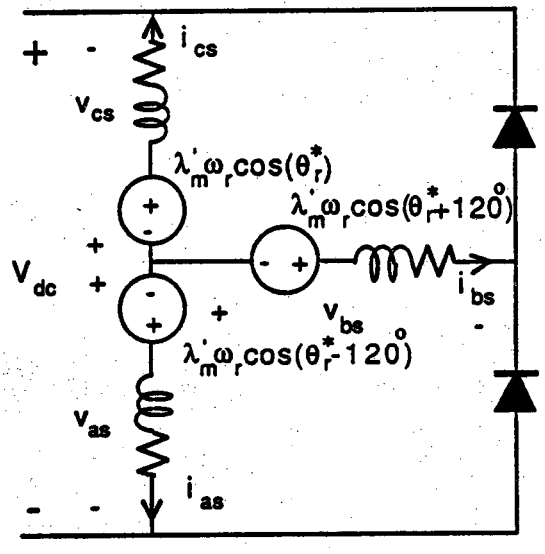

Figure 4.4 Fig 4.3, Rearranged

switching intervals may be expressed mathematically as

$$\vec{f}\left(\Theta_r + \frac{\pi}{3}\right) = \begin{bmatrix} 0 & -1 & 0 \\ 0 & 0 & -1 \\ -1 & 0 & 0 \end{bmatrix} \vec{f}\left(\Theta_r\right) \tag{4.1}$$

where $\vec{f}$ can represent any abcs voltage, current, or flux linkage quantity.

Current Waveforms For Constant Speed Operation

It has just been shown that if one can describe abcs waveforms in BSI II then one can describe the waveforms in all other BSI as well. This section sets forth and solves the differential equations which apply during BSI II.

Because of the switching nature of the diodes there are two sets of differential equations which describe BSI II. During N or P intervals

$$\rho \begin{bmatrix} i_{as} \\ i_{bs} \\ i_{cs} \end{bmatrix} = -\frac{r_s}{L_s} \begin{bmatrix} i_{as} \\ i_{bs} \\ i_{cs} \end{bmatrix} + \frac{1}{L_s} \begin{bmatrix} v_{as} - \omega_r \lambda'_r \cos\left(\Theta'_r - \phi + \frac{\pi}{6}\right) \\ v_{bs} - \omega_r \lambda'_m \sin\left(\Theta'_r - \phi\right) \\ v_{cs} - \omega_r \lambda'_m \cos\left(\Theta'_r - \phi + \frac{5\pi}{6}\right) \end{bmatrix} \tag{4.2}$$

In order to provide a more convenient interval, (4.2) has been shifted so that BSI II starts at $\Theta_r' = 0$ and ends at $\Theta_r' = \frac{\pi}{3}$. The relation between Θ_r and Θ_r' is that $\Theta_r = \Theta_r' + \frac{\pi}{6} - \phi$.

The stator voltages in (4.2) are as follow.

$$V_{abcs} = \begin{bmatrix} \frac{V_{dc}}{3} \\ \frac{V_{dc}}{3} \\ -\frac{2V_{dc}}{3} \end{bmatrix} \quad \text{N Interval} \tag{4.3}$$

$$V_{abcs} = \begin{bmatrix} \frac{2V_{dc}}{3} \\ -\frac{V_{dc}}{3} \\ -\frac{V_{dc}}{3} \end{bmatrix} \quad \text{P Interval} \tag{4.4}$$

Assuming constant speed, the differential equation described by (4.2) is linear, first order, and uncoupled. The solution is

$$i_{as}\left(t,t_o\right) = i_{as}\left(t_o\right)e^{-\frac{r_s}{L_s}\left(t-t_o\right)} + \frac{v_{as}}{r_s}\left[1 - e^{-\frac{r_s}{L_s}\left(t-t_o\right)}\right] \tag{4.5}$$

$$+ \frac{\omega_r\lambda'_m}{r_s^2 + \omega_r^2 L_s^2}\left[\omega_r L_s \sin\left(\omega_r t_o + \frac{\pi}{6} - \phi\right) + r_s\cos\left(\omega_r t_o + \frac{\pi}{6} - \phi\right)\right]e^{-\frac{r_s}{L_s}\left(t-t_o\right)}$$

$$- \frac{\omega_r\lambda'_m}{r_s^2 + \omega_r^2 L_s^2}\left[\omega_r L_s \sin\left(\omega_r t + \frac{\pi}{6} - \phi\right) + r_s\cos\left(\omega_r t + \frac{\pi}{6} - \phi\right)\right]$$

$$i_{bs}\left(t, t_o\right) = i_{bs}\left(t_o\right)e^{-\frac{r_s}{L_s}\left(t - t_o\right)} + \frac{v_{bs}}{r_s}\left[1 - e^{-\frac{r_s}{L_s}\left(t - t_o\right)}\right] \tag{4.6}$$

$$+ \frac{\omega_r \lambda'_m}{r_s^2 + \omega_r^2 L_s^2}\left[\omega_r L_s \cos\left(\omega_r t - \phi\right) - r_s \sin\left(\omega_r t - \phi\right)\right]$$

$$- \frac{\omega_r \lambda'_m}{r_s^2 + \omega_r^2 L_s^2}\left[\omega_r L_s \cos\left(\omega_r t_o - \phi\right) - r_s \sin\left(\omega_r t_o - \phi\right)\right] e^{-\frac{r_s}{L_s}\left(t - t_o\right)}$$

$$i_{cs}\left(t, t_o\right) = -i_{as}\left(t, t_o\right) - i_{bs}\left(t, t_o\right) \tag{4.7}$$

During Z intervals, (4.8) applies. The solution of (4.8) is given by (4.9) - (4.11).

$$\rho\begin{bmatrix} i_{as} \\ i_{bs} \\ i_{cs} \end{bmatrix} = -\frac{r_s}{L_s}\begin{bmatrix} i_{as} \\ i_{bs} \\ i_{cs} \end{bmatrix} + \frac{1}{L_s}\begin{bmatrix} \frac{V_{dc}}{2} - \frac{\sqrt{3}}{2}\omega_r \lambda'_m \cos\left(\Theta_r' - \phi\right) \\ 0 \\ -\frac{V_{dc}}{2} + \frac{\sqrt{3}}{2}\omega_r \lambda'_m \cos\left(\Theta_r' - \phi\right) \end{bmatrix} \tag{4.8}$$

$$i_{as}\left(t, t_o\right) = i_{as}\left(t_o\right)e^{-\frac{r_s}{L_s}\left(t - t_o\right)} + \frac{V_{dc}}{2rs}\left[1 - e^{-\frac{r_s}{L_s}\left(t - t_o\right)}\right] \tag{4.9}$$

$$+ \frac{\omega_r \lambda'_m}{r_s^2 + \omega_r^2 L_s^2}\,\frac{\sqrt{3}}{2}\left[\omega_r L_s \sin\left(\omega_r t_o - \phi\right) + r_s \cos\left(\omega_r t_o - \phi\right)\right] e^{-\frac{r_s}{L_s}\left(t - t_o\right)}$$

$$- \frac{\omega_r \lambda'_m}{r_s^2 + \omega_r^2 L_s^2}\,\frac{\sqrt{3}}{2}\left[\omega_r L_s \sin\left(\omega_r t - \phi\right) + r_s \cos\left(\omega_r t - \phi\right)\right]$$

$$i_{bs}\left(t, t_o\right) = 0 \tag{4.10}$$

$$i_{cs}\left(t, t_o\right) = -i_{as}\left(t, t_o\right) \tag{4.11}$$

At this time it is appropriate to review what has been done. First of all, it has been shown that it is only necessary to consider BSI II to completely describe inverter operation. Secondly, the differential equations which describe BSI II have been laid out and solved for N,P and Z intervals. The next step will be to utilize the analytical solution just derived to formulate a simulation technique. This formulation is the subject of the next chapter.

CHAPTER 5
SIMULATION OF STEADY STATE PERFORMANCE

One method of calculating the current waveforms for steady state operation of the brushless dc 120° inverter system is to solve the appropriate differential equations numerically. This requires numerical integration which is computationally slow due to the large number of iterations required as a result of the small stator time constant and the discontinuous nature of the forcing functions.

The method presented here overcomes this difficulty by utilizing the analytical solution to the differential equations laid out in the previous chapter to avoid numerical integration and thereby greatly reduce computation time.

The Algorithm

The algorithm to compute the current waveforms for steady state operation is as follows. First of all, calculate the current waveforms on BSI II. Secondly, use the symmetry condition expressed by (4.1) to find the current waveforms on all other BSI.

Calculation of the current waveforms on BSI II is dependent upon an iterative process to calculate the initial currents in BSI II. Given an estimate of the initial currents in BSI II the corresponding value of the final currents in BSI II is found. Using the symmetry condition expressed by (4.1) the final currents are used to form a refined estimate for the initial currents. The process repeats until the refined estimate for the the initial currents calculated from (4.1) at the end of an iteration becomes sufficiently close to the estimate for the initial currents used at the beginning of that iteration.

In order to do this, however, it is necessary to be able to calculate the currents at the end of an iteration from the currents at the beginning of an iteration. As has been alluded to, this will be done by utilizing the analytical solution of the differential equations which apply during BSI II. However, the

application of the solution of the differential equations is not straight forward since BSI II consists of N,P, and Z intervals each of which is described by a different set of differential equations. To remedy the situation, an iterative method is employed as follows. First, given the initial currents for BSI II and knowledge of the location of the domains the initial type of interval, N,P or Z, is determined. Using this information, the location of and the currents at the end of the first N,P or Z interval are found. Once the currents at the end of the first N,P or Z interval are found, the type of the second interval, N,P or Z, is determined. Next, the currents at the end of the second N,P, or Z interval are calculated. An identical set of operations is performed for the third interval and the process keeps repeating until the end of BSI II is reached.

The final problem to be addressed is the determination of the end of a given interval. For a Z interval, the end of the interval comes at the beginning of the next Z-N or Z-P domain, or the end of BSI II, whichever comes first. In the case of a N or P interval, the end of the interval is found by searching for the zero crossing of i_{bs}.

Computing Block Diagram

A block diagram for the simulation technique to be described is shown in Fig. 5.1. The diagram is somewhat cryptic for simplicity; therefore each block of interest has been labeled with a capital letter which corresponds to a section of the following description labeled with the same letter.

Block A

The first step in the algorithm is to identify the Z-N and Z-P domains, which can be found using (3.17) or (3.18). Since the simulation is most conveniently done it terms of Θ_r' rather that Θ_r, (5.1) and (5.2) express (3.17) and (3.18) in terms of Θ_r'

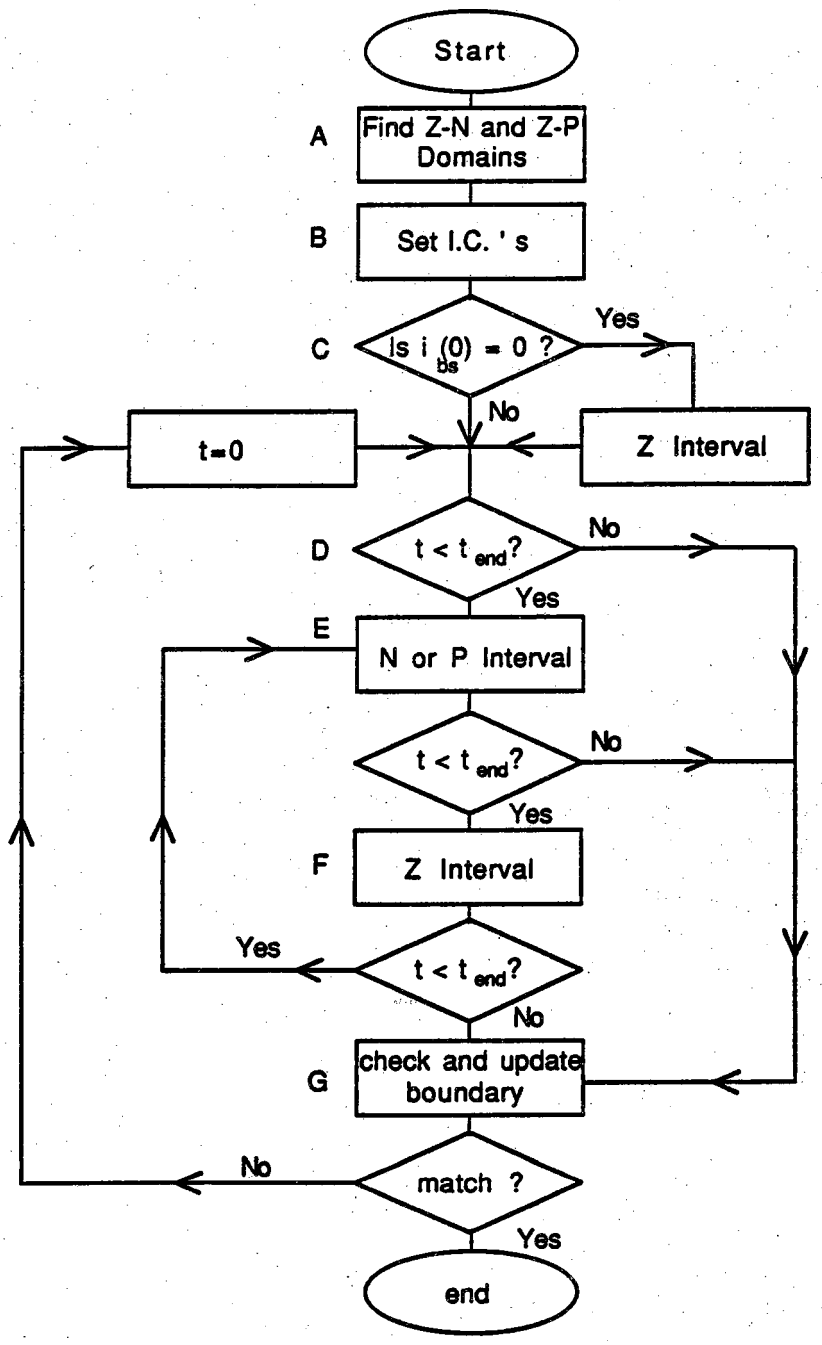

Figure 5.1 Computing Block Diagram

$$\sin\left(\Theta_r' - \phi\right) > \frac{V_{dc}}{3\lambda_m'\omega_r} \qquad \text{Z-N Domain} \qquad (5.1)$$

$$\sin\left(\Theta_r' - \phi\right) < -\frac{V_{dc}}{3\lambda_m'\omega_r} \qquad \text{Z-P Domain} \qquad (5.2)$$

Block B

The second step of the algorithm is to set all initial conditions. Time zero is defined to occur at the beginning of BSI II. Therefore t and Θ_r' are initially set to zero. These two quantities are synonymous since for constant speed $\Theta_r' = \omega_r t$.

Setting the initial value of the currents is dependent upon the context in which the algorithm is being used. Normally, all the initial currents are set equal to zero for the first iteration. However, if the purpose of the user is to generate a torque speed curve by repeated execution of the algorithm at progressively higher speeds it is economical to choose the initial conditions for a given run to be those of the previous run since this will provide an estimate for the new initial conditions which will lead to faster convergence.

Block C

If $i_{bs} = 0$ then the next interval is of type Z, otherwise the next interval is of type N or P.

Block D

This block tests for the completion of the switching interval. Note that $t_{end} = \frac{\pi}{3\omega_r}$.

Block E

This block can be entered under four possible conditions. These are: $i_{bs}<0$, a Z-N transition with $i_{bs} = 0$, $i_{bs}>0$, or Z-P transition with $i_{bs} = 0$. In any case, this block determines the end of the N or P interval and the value of

the currents at the end of the interval by using (4.5) - (4.7). In the first two entry conditions an N interval occurs and (4.3) applies; in the last two cases a P interval occurs and (4.4) applies. When utilizing (4.5)-(4.7) we must realize that t_o refers to the beginning of the N,P, or Z interval being traversed. The goal is to determine the the time t at which the N or P interval ends and to evaluate the currents at the end of the N or P interval.

The determination of the end of the N or P interval is done by finding the zero crossing of i_{bs}. A search method is employed to accomplish this. From the start of the N or P interval, i_{bs} is evaluated at time increments spaced apart by one tenth of the time duration of BSI II until the direction of i_{bs} does not agree with the characteristics of the N or P interval or until the end of BSI II is reached. Once the segment of time during which the zero crossing must occur is determined, i_{bs} is evaluated at time increments one fifth of the length of the time increment previously used within this segment in order to place the end of the N or P interval in an even smaller segment of time. The process repeats until the segment of time during which the zero crossing occurs has been made sufficiently small. With this method, 50 evaluations of i_{bs} will result in a maximum rotor position error of $\frac{\pi}{11718750}$ of a radian in the zero crossing. To achieve similar accuracy with a strictly numerical simulation would require 3906250 iterations within BSI II. Note that this search is subject to $t<t_{end}$.

Once t is known, the currents may be calculated. These currents become the initial currents for the next N,P or Z interval. Also t_o is set equal to t for calculation within the next N,P or Z interval.

There are two other calculations which may be performed in this block after the algorithm converges. The first is that once the algorithm converges to a solution one may wish evaluate the currents at regularly spaced increments of time for the purposes of graphical output. Secondly, one may wish to evaluate the integral of the v_{qs} and v_{ds} over the N or P interval in order to compute the average of these quantities over BSI II. From this, the average torque may be obtained as detailed in a later section.

Block F

Block F is similar to block E except that it is for a Z interval as opposed to a N or P interval. Block F begins with a check to make sure a Z-N or Z-P transition is not occurring - if it is the algorithm exits block F. Otherwise,

block F calculates the currents at the end of the Z interval using (4.9) - (4.11) and updates t as with Block E. Note that, unlike the end of the N or P interval, the end of the Z interval is known immediately and is either the beginning of the next Z-N or Z-P domain or the end of BSI II, whichever occurs first. Block F also contains the same auxiliary calculations as block E such as waveform evaluation and calculations leading to the average torque.

Block G

The function of block G is to calculate an improved estimate for the initial BSI II currents based upon the value of the final BSI II currents just calculated and to test for convergence of the algorithm. At the end of BSI II the currents of equation (5.3) are known. Applying the inverse of (4.1) we see that the corresponding initial conditions are given by (5.4). Thus it is possible to continue on with a refined solution. By comparing this new estimate of the initial conditions to the previous estimate the algorithm can determine if convergence has been achieved. Once the algorithm converges a flag is set which causes a final pass through BSI II during which auxiliary calculations such as the integration v_{qs}^{r} and v_{ds}^{r} or the construction of waveforms are performed. This has not been shown in block diagram for the purpose of simplicity.

$$i_{abcs}\left(t_{tend}\right) = \begin{bmatrix} i_{asf} \\ i_{bsf} \\ i_{csf} \end{bmatrix} \tag{5.3}$$

$$i_{abcs}\left(0\right) = \begin{bmatrix} -i_{csf} \\ -i_{asf} \\ -i_{bsf} \end{bmatrix} \tag{5.4}$$

Average Torque Calculations

Calculation of the average torque begins with the symmetry condition expressed by (4.1). Applying the transformation to the rotor reference frame to (4.1) we have

$$\vec{f}^{r}_{qdos}\left(\Theta_r + \frac{\pi}{3}\right) = K^r_s\left(\Theta_r + \frac{\pi}{3}\right)\begin{bmatrix} 0 & -1 & 0 \\ 0 & 0 & -1 \\ -1 & 0 & 0 \end{bmatrix}\left(K^r_s\left(\Theta_r\right)\right)^{-1}\vec{f}^{r}_{qdos} \tag{5.5}$$

Equation (5.5) reduces to (5.6) which implies that for steady state conditions, the qdos variables are periodic with a time period corresponding to one switching interval.

$$\vec{f}^{r}_{qdos}\left(\Theta_r + \frac{\pi}{3}\right) = \vec{f}^{r}_{qdos}\left(\Theta_r\right) \tag{5.6}$$

Integrating (2.9), (2.10), and (2.11) over one BSI in rotor position and dividing by $\frac{\pi}{3}$ we obtain

$$\bar{v}^{r}_{qs} = r_s\bar{i}^{r}_{qs} + \omega_r L_s\bar{i}^{r}_{ds} + \omega_r\lambda_m' \tag{5.7}$$

$$\bar{v}^{r}_{ds} = r_s\bar{i}^{r}_{ds} - \omega_r L_s\bar{i}^{r}_{qs} \tag{5.8}$$

$$\bar{T}_e = \left(\frac{3}{2}\right)\left(\frac{P}{2}\right)\lambda_m'\bar{i}^{r}_{qs} \tag{5.9}$$

where barred quantities represent average values. Equations (5.7) and (5.8) can be solved for $\bar{i}^{r}_{qs}$ which can then be substituted into (5.9) to give

$$\bar{T}_e = \left(\frac{3}{2}\right)\left(\frac{P}{2}\right)\lambda'_m \frac{r_s}{r_s^2 + \omega_r^2 L_s^2}\left(\bar{v}^r_{qs} - \frac{L_s}{r_s}\bar{v}^r_{ds}\omega_r - \lambda'_m\omega_r\right) \tag{5.10}$$

for the average torque in terms of $\bar{v}^r_{qs}$ and $\bar{v}^r_{ds}$. In order to efficiently calculate these quantities the expressions for the integral of v^r_{qs} and v^r_{ds} during the N,P and Z intervals of BSI II are needed. For the N and P intervals, the v_{abcs} variable are constant. Applying (2.7) and integrating gives

$$\int_{\theta'_{ro}}^{\theta'_r} v^r_{qs} d\theta'_r = 1.1547 v_{as}\left[\sin\left(\theta_r' - \phi\right) - \sin\left(\theta_{ro}' - \phi\right)\right] \tag{5.11}$$

$$+ 1.1547 v_{bs}\left[\sin\left(\theta_r' - \phi - \frac{\pi}{3}\right) - \sin\left(\theta_{ro}' - \phi - \frac{\pi}{3}\right)\right]$$

$$\int_{\theta'_{ro}}^{\theta_r} {}' v^r_{ds} d\theta'_r = 1.1547 v_{as}\left[\cos\left(\theta_{ro}' - \phi\right) - \cos\left(\theta'_r - \phi\right)\right] \tag{5.12}$$

$$+ 1.1547 v_{bs}\left[\cos\left(\theta_{ro}' - \phi - \frac{\pi}{3}\right) - \cos\left(\theta_r' - \phi - \frac{\pi}{3}\right)\right]$$

Similar expressions may be derived for Z interval. However, in the case of the Z interval the applied voltages contain the back emf of the open circuited phase. Transforming the appropriate expressions into the rotor reference frame and integrating result in

$$\int_{\Theta'_{ro}}^{\Theta'_r} v^r_{qs} d\Theta'_r = .57737 V_{dc}\left[\sin\left(\Theta'_r - \phi\right) - \sin\left(\Theta'_{ro} - \phi\right)\right] \qquad (5.13)$$

$$+ .5\lambda'_m \omega_r \left[\Theta'_r - \Theta'_{ro}\right]$$

$$- .25\lambda'_m \omega_r \left[\sin\left(2\left(\Theta'_r - \phi\right)\right) - \sin\left(2\left(\Theta'_{ro} - \phi\right)\right)\right]$$

$$\int_{\Theta'_{ro}}^{\Theta'_r} v^r_{ds} d\Theta'_r = .57737 V_{dc}\left[\cos\left(\Theta'_{ro} - \phi\right) - \cos\left(\Theta'_r - \phi\right)\right] \qquad (5.14)$$

$$+ .25\lambda'_m \omega_r \left[\cos\left(2\left(\Theta'_r - \phi\right)\right) - \cos\left(2\left(\Theta'_{ro} - \phi\right)\right)\right]$$

Once the integrals of v^r_{qs} and v^r_{ds} over BSI II are known, dividing by $\frac{\pi}{3}$ results in $\overline{v}^r_{qs}$ and $\overline{v}^r_{ds}$.

CHAPTER 6
OPERATIONAL MODES

One advantage of the analytical/numerical simulation is that the N,P and Z intervals are explicately recognized within BSI II. In this chapter we will take advantage of this to classify inverter behavior into different modes based on a qualitative history of BSI II in terms of the sequence of N,P and Z intervals. This classification results in a better understanding of inverter operation, and provides a means of determining the conditions under which the the open circuit voltage may be utilized to determine the rotor position. In addition, the information set forth in this chapter establishes guidelines for the development of approximate transfer functions.

Classification Scheme

The classification of inverter operation into modes is based on the sequence of N,P and Z intervals within BSI II. A convenient nomenclature is to designate the mode by concatenating the letters "N","P", and "Z" in the sequence in which the corresponding N,P, and Z intervals occurred during BSI II. As an example, consider Fig 3.2. BSI II consists of an N interval followed by a Z interval and finally another N interval. This mode of inverter operation is classified as NZN. Similarly, for the conditions in Fig 3.4, operation is NPZ mode.

Fig. 6.1. is a map showing the occurrence of modes in the ω_r - ϕ plane. The machine parameters are given in Appendix A. For the machine parameters used nine modes occurred, six of which were capable of producing positive torque.

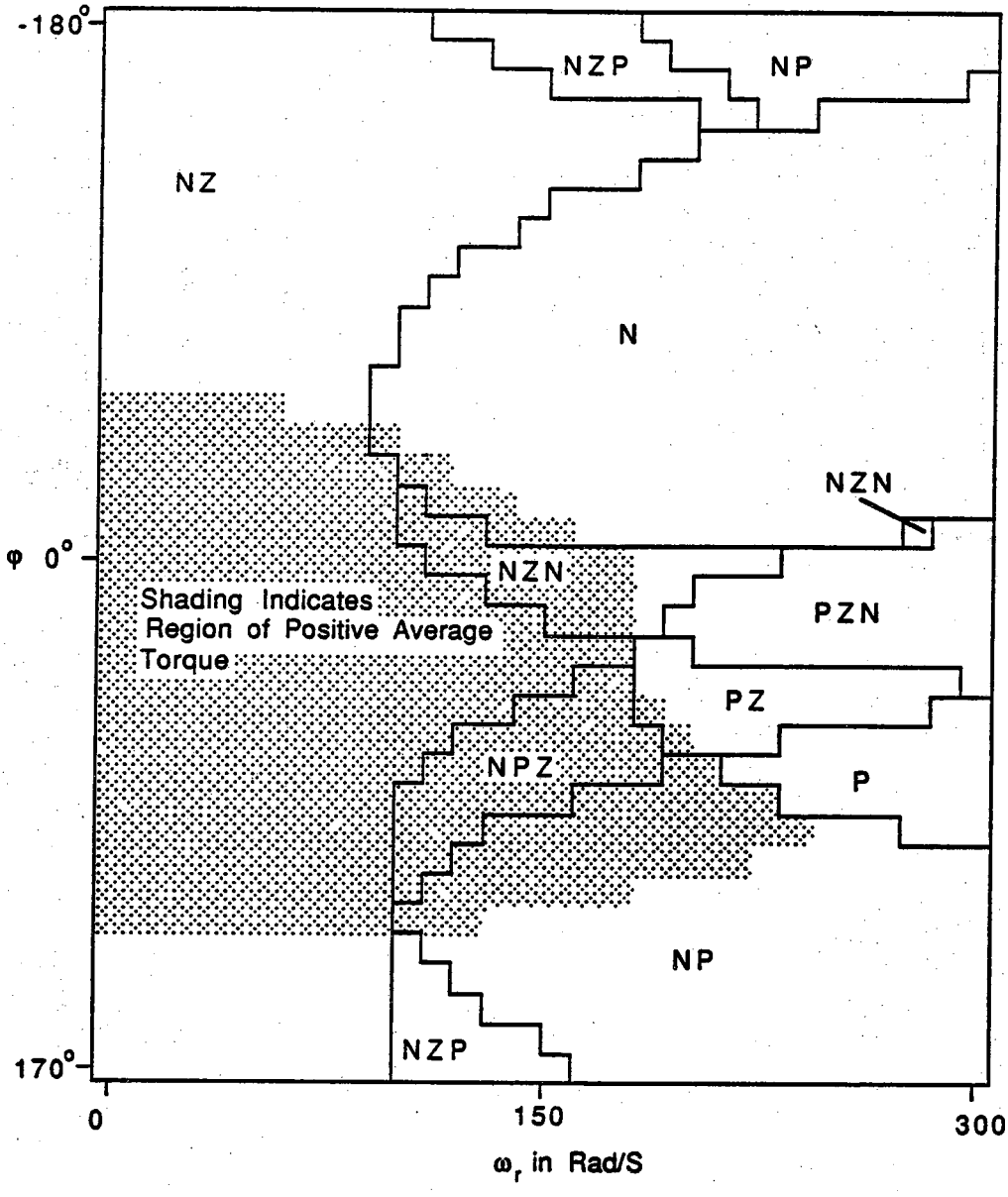

Figure 6.1 Modes on the ω_r - ϕ Plane

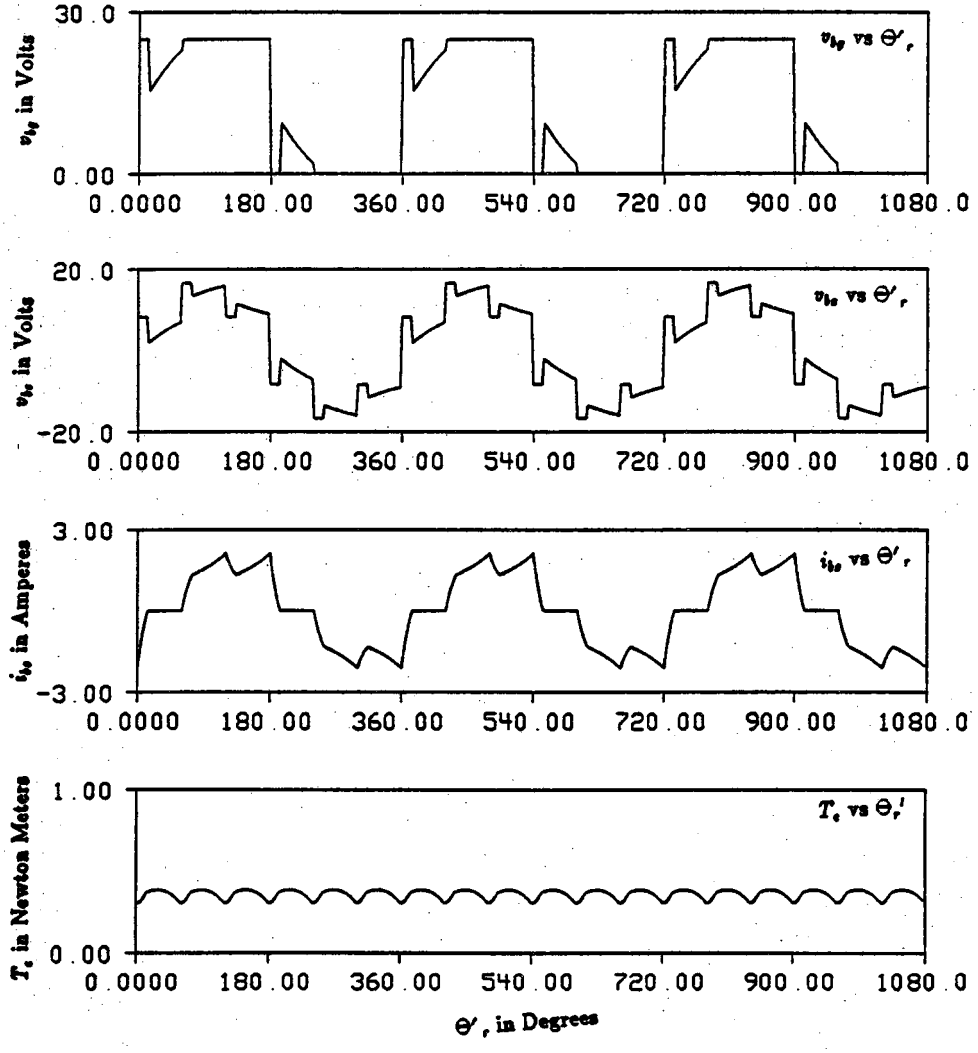

Figure 6.2 The NZ Mode

The NPZ mode

In NPZ operation the N interval terminates in a Z-P domain, which result in a Z-P transition and therefore a P interval. The P interval cannot end until Θ_r leaves the Z-P domain. Once Θ_r does leave the Z-P domain, i_{bs} must decrease. Once i_{bs} becomes zero a Z interval begins and continues until the end of BSI II.

The N Mode

The N mode of operation results when most of BSI II lies within an Z-N domain so that the current does not go to zero. Hence the NZ mode does not occur. It is interesting to note that if operation is N type then the situation is identical to that of a brushless dc with a 180° inverter system.

The NZN Mode

The NZN mode is similar to the NZ mode except that a a Z-N transition occurs during the Z interval as the result of Θ_r entering a Z-N domain. The net result is a second N interval.

The NP Mode

In the case of the NP mode, the Z-P domain occupies enough of BSI II to prevent i_{bs} from returning to zero which would yield a NPZ mode.

The PZ Mode

As the speed increases for a given applied voltage so does the back emf which causes the currents to decrease in magnitude. With this decrease in current, i_{bs} becomes less negative at the beginning of BSI II, resulting in a shorter initial N interval. Eventually, as speed increases, the back emf in BSI I causes the initial i_{bs} in BSI II to become positive which causes an initial P interval.

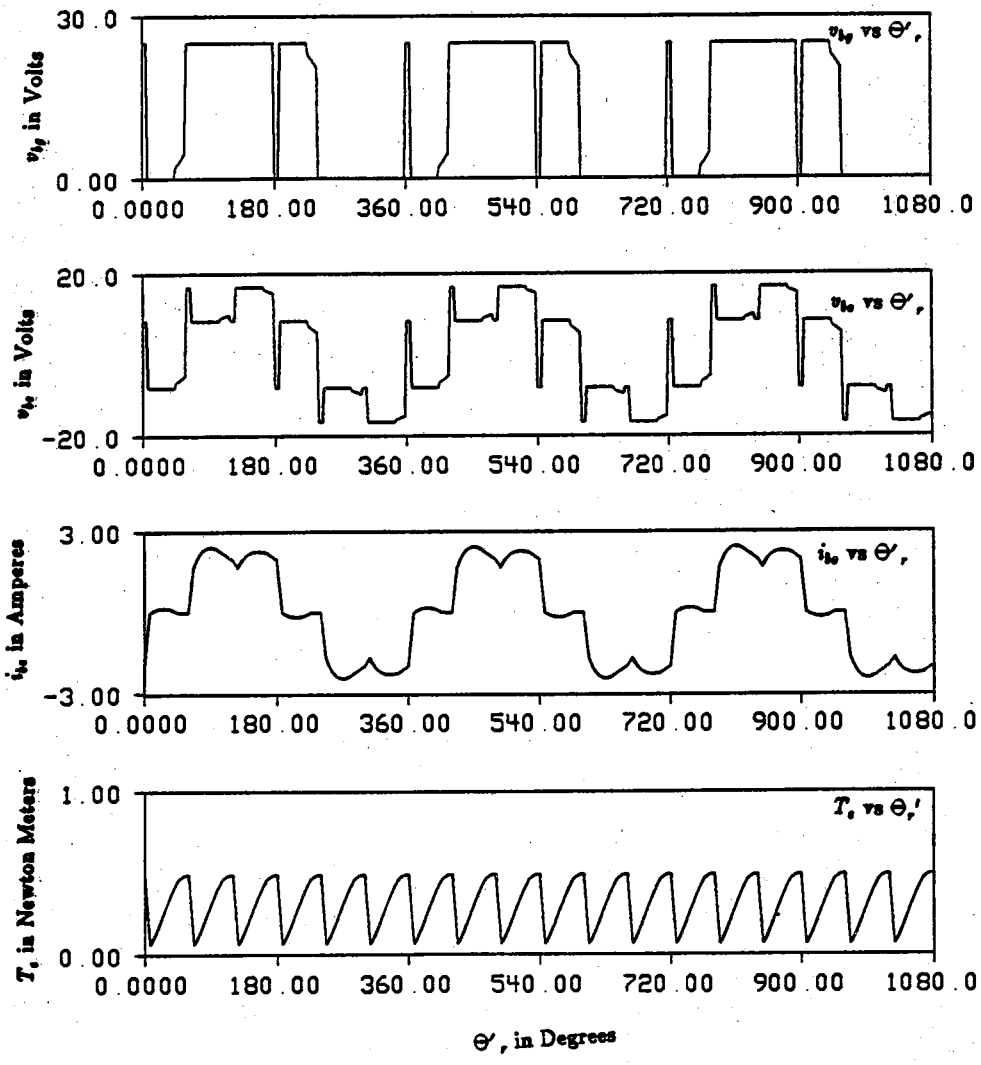

Figure 6.3 The NPZ Mode

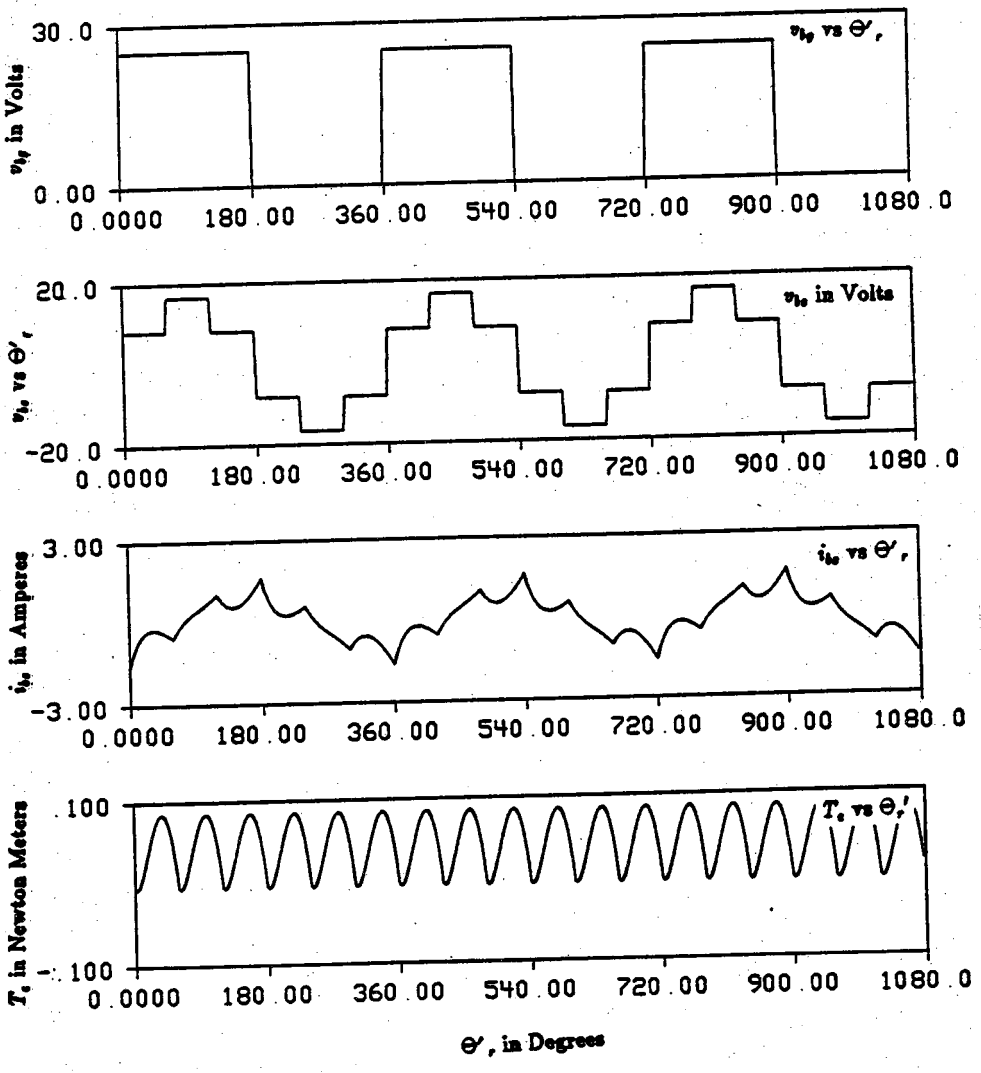

Figure 6.4 The N Mode

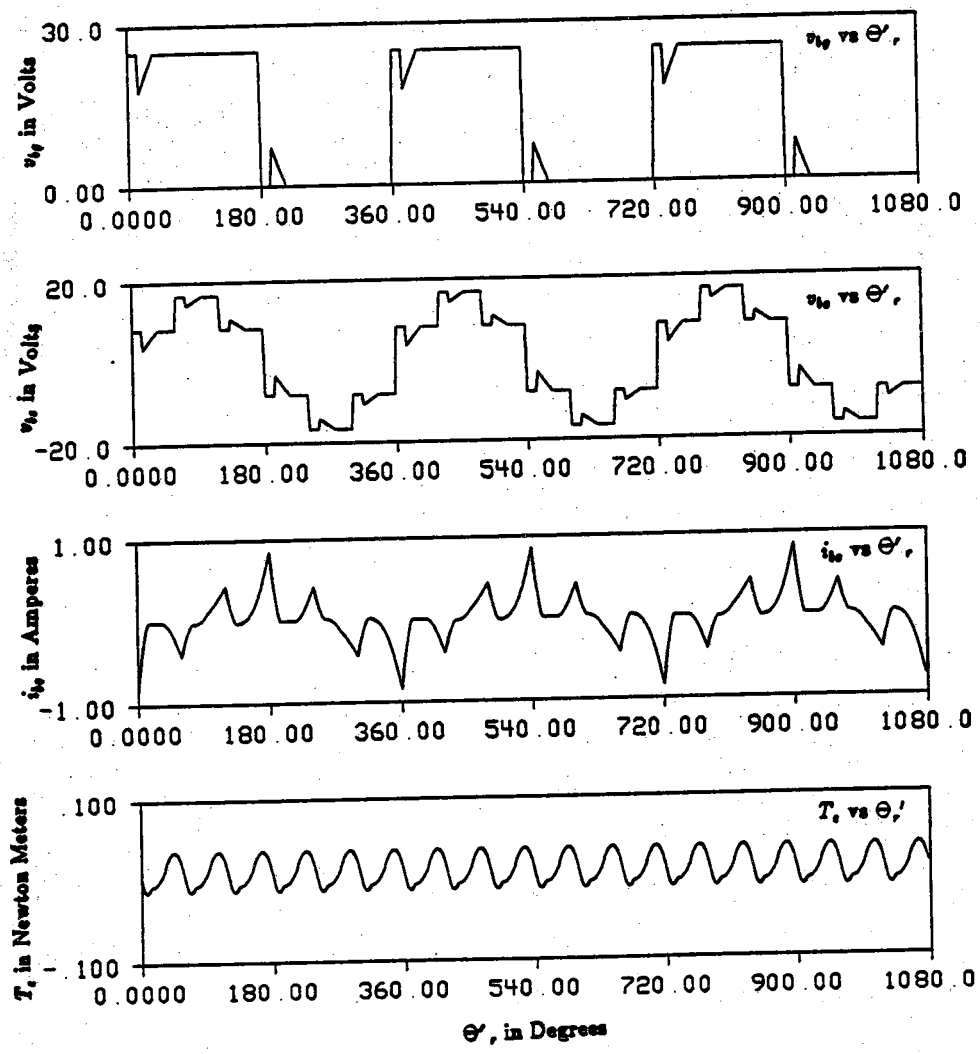

Figure 6.5 The NZN Mode

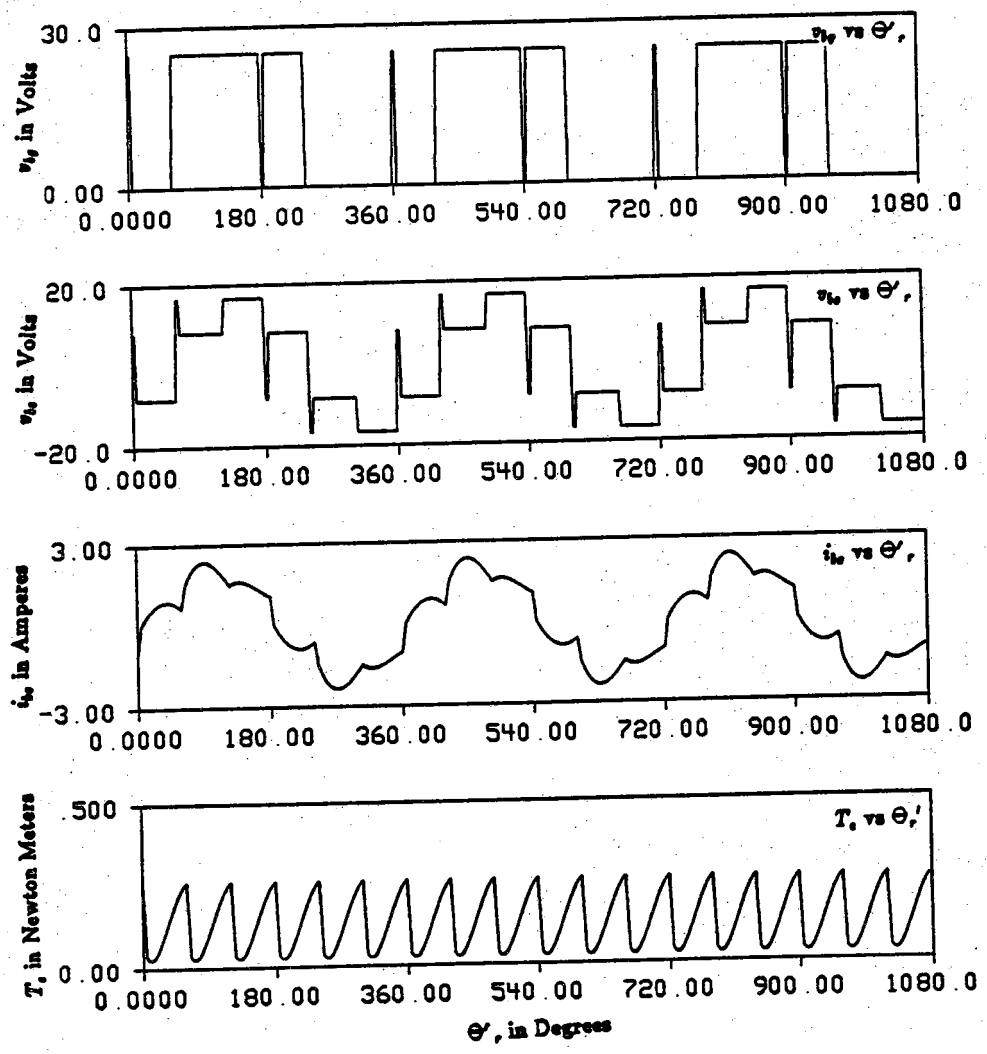

Figure 6.6 The NP Mode

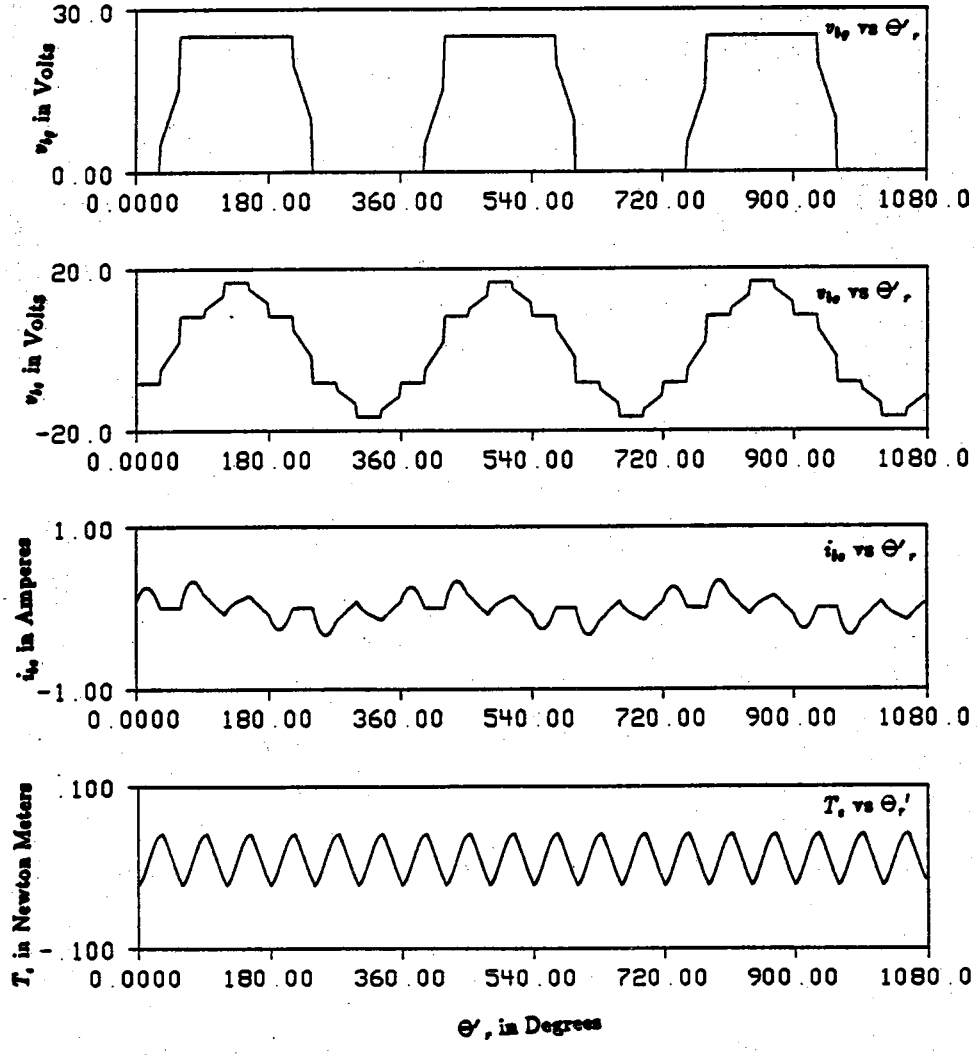

Figure 6.7 The PZ Mode

Inverter Behavior vs Frequency

When considering the various modes it is found that one mode is often the extension of another. Relationships between the modes are best illustrated by an interval map such as Figs. 6.8 - 6.11. Consider Fig. 6.8 which is a interval map for $\phi = 0$. The vertical axis represents Θ_r' which progresses from 0° to 60° in the course of BSI II. The horizontal axis represents ω_r. The map is interpreted as follows. For a given speed, say $\omega_r = 187.5$ start at $\Theta_r' = 0$ which is point A and move up vertically until the intersection with the first curve at point B. The interpretation is that from $\Theta_r' = A$ to $\Theta_r' = B$ an N interval existed. Proceeding upward until the second intersection is reached at point C we find that the N interval is followed by a Z interval which occurs from $\Theta_r' = B$ to $\Theta_r' = C$. Moving upward again the Z interval is followed by another N interval which begins at $\Theta'_r = C$ and ends at the termination of BSI II.

Collectively, Figs. 6.8 - 6.11 are the interval maps for $\phi = 0°$, $30°$, $60°$, and $90°$, respectively. From Fig 6.8. we see that for $\phi = 0°$ operation is NZ mode for rotor speeds from 0 to 115 Rad/S. The large arc at the top left hand corner is the boundary for the Z-N domain. Along this arc Z-N transitions occur. Therefore, from $\omega_r = 115$ Rad/S to $\omega_r = 250$ Rad/S operation is classified as NZN mode. At ω_r=250Rad/S the initial current i_{bs} changes sign and operation becomes classified as PZN mode.

Fig. 6.9. depicts the interval map for $\phi = 30°$. Note that the Z-N and Z-P domains are symmetrical about $\Theta'_r = 30°$, as one expects from Fig 3.3. The Z-P domain is indicated in a dashed line in this figure since Z-P transitions do not occur along this boundary since i_{bs} must be zero for a Z-P transition to occur. In Fig 6.10 and 6.11, the Z-P domain becomes larger as ϕ is increased. This can be understood by examining the relationship between the intersection of the domains with BSI II as a function of ϕ in Fig 3.3. In both cases, at the NZ mode occurs at low speed operation; however as speed increases a rapidly enlarging P interval causes the NPZ mode of operation. As ω_r becomes even larger in Fig 6.10 operation becomes PZ and finally the P mode. In the $\phi = 90°$ case (Fig. 6.11), the NPZ mode is followed by the NP and then P mode of operation as rotor speed increases.

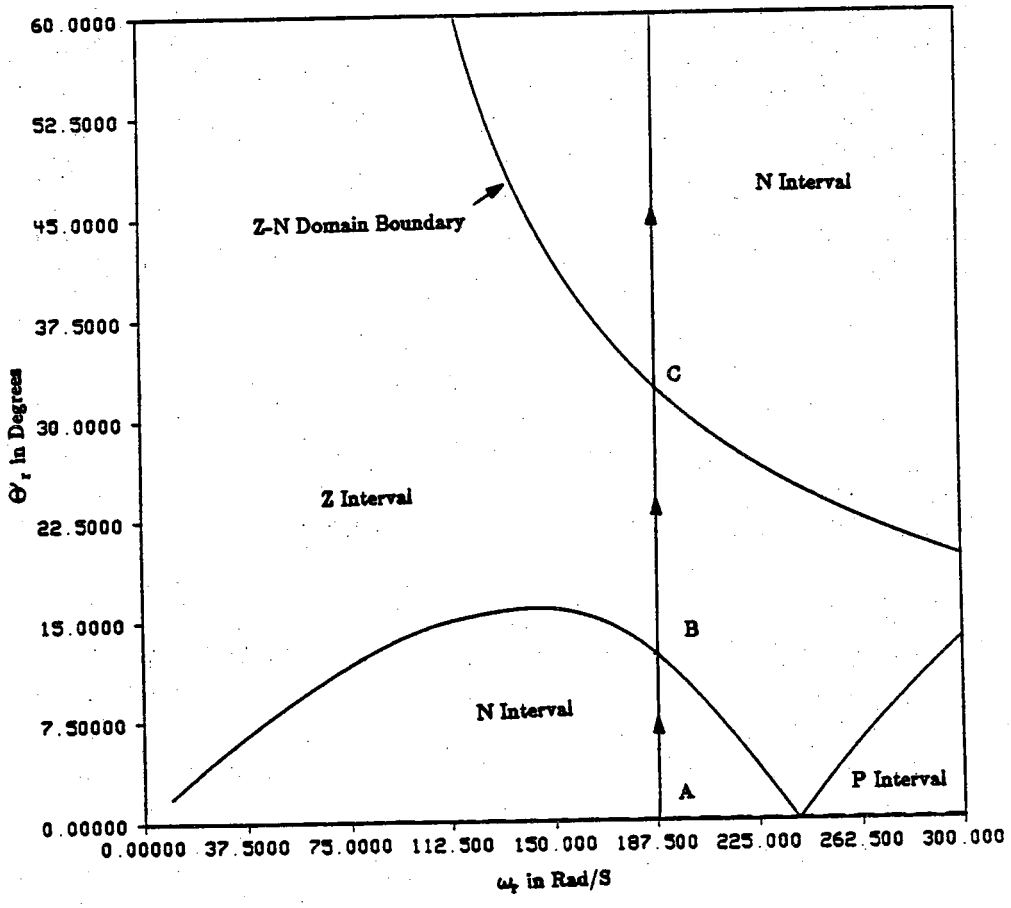

Figure 6.8 Interval Map for $\phi = 0^{\circ}$

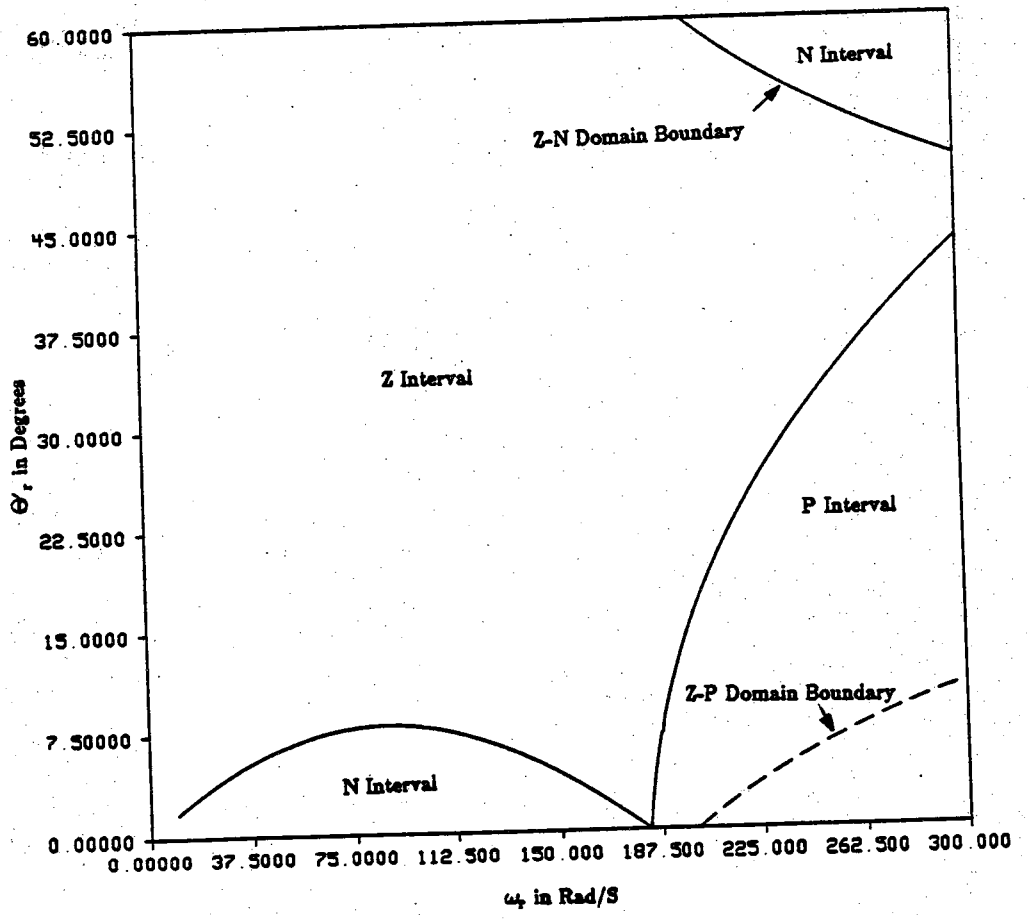

Figure 6.9 Interval Map for $\phi = 30°$

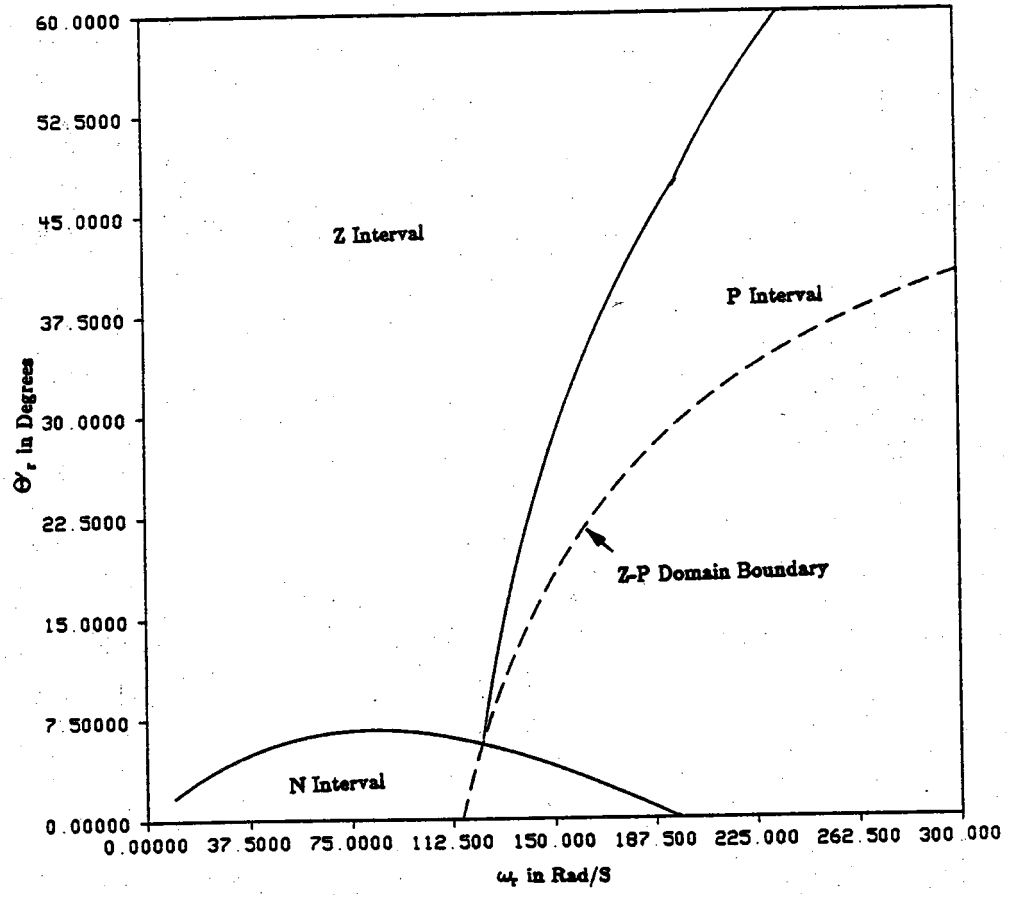

Figure 6.10 Interval Map for $\phi = 60^{\circ}$

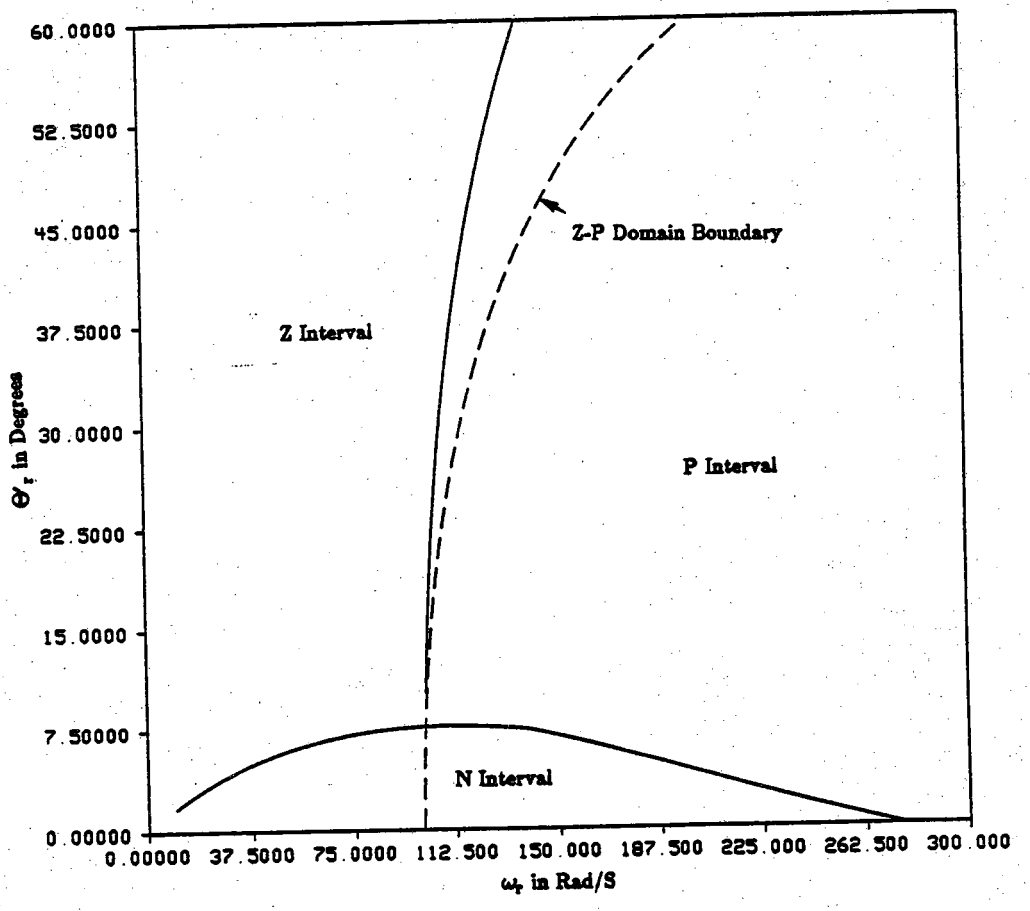

Figure 6.11 Interval Map for $\phi = 90°$

voltage will be $\frac{1}{2} V_{dc}$. Using this fact, along with (3.7)-(3.9) we are able to fill in the question marks in Table 3.2, and to include v_{as}, v_{bs}, and v_{cs}. This information is given in Table 7.1.

Table 7.1 120° Inverter Operation with Resistive Load

BSI	$\Theta_r - \phi$	Transistors On	v_{ag}	v_{bg}	v_{cg}	v_{as}	v_{bs}	v_{cs}
I	0°	1,6	V_{dc}	0	$\frac{1}{2} V_{dc}$	$\frac{1}{2} V_{dc}$	$-\frac{1}{2} V_{dc}$	0
II	60°	1,2	V_{dc}	$\frac{1}{2} V_{dc}$	0	$\frac{1}{2} V_{dc}$	0	$-\frac{1}{2} V_{dc}$
III	120°	2,3	$\frac{1}{2} V_{dc}$	V_{dc}	0	0	$\frac{1}{2} V_{dc}$	$-\frac{1}{2} V_{dc}$
IV	180°	3,4	0	V_{dc}	$\frac{1}{2} V_{dc}$	$-\frac{1}{2} V_{dc}$	$\frac{1}{2} V_{dc}$	0
V	240°	4,5	0	$\frac{1}{2} V_{dc}$	V_{dc}	$-\frac{1}{2} V_{dc}$	0	$\frac{1}{2} V_{dc}$
VI	300°	5,6	$\frac{1}{2} V_{dc}$	0	V_{dc}	0	$-\frac{1}{2} V_{dc}$	$\frac{1}{2} V_{dc}$

It is possible to expand v_{as}, v_{bs}, and v_{cs} into a Fourier series in Θ_r. By neglecting all harmonics and transforming the fundamental to the rotor reference frame we obtain (7.1) and (7.2).

$$\overrightarrow{v}^{r}_{qs} = \frac{\sqrt{3}}{\pi} V_{dc} \cos\left(\phi - \frac{\pi}{6}\right) \tag{7.1}$$

$$\overrightarrow{v}^{r}_{ds} = -\frac{\sqrt{3}}{\pi} V_{dc} \sin\left(\phi - \frac{\pi}{6}\right) \tag{7.2}$$

A comparison of (7.1) and (7.2) with (2.13) and (2.14) suggests the equivalence of $\phi - \frac{\pi}{6}$ to α, at least for low speeds.

Approximation C

Often BSI II consists of a relatively brief N interval followed by a Z interval. This is particularly the case for $\phi = 30°$ at low to moderate speeds as shown in Fig 6.9. If the N interval is neglected then the average value of v_{qs}^r and v_{ds}^r may be found by evaluating (5.13) and (5.14) from $\Theta_r' = 0$ to $\Theta_r' = \frac{\pi}{3}$ and dividing by the length of the switching interval which is $\frac{\pi}{3}$. The result is given by (7.6) and (7.7).

$$\bar{v}_{qs}^r = \frac{\sqrt{3}}{\pi} V_{dc} \sin\left(\phi + \frac{\pi}{3}\right) + \frac{1}{2}\omega_r \lambda_m' \left[1 - \frac{3\sqrt{3}}{2\pi} \cos\left(2\phi - \frac{\pi}{3}\right)\right] \tag{7.6}$$

$$\bar{v}_{ds}^r = \frac{\sqrt{3}}{\pi} V_{dc} \cos\left(\phi + \frac{\pi}{3}\right) + \frac{3\sqrt{3}}{4\pi} \omega_r \lambda_m' \sin\left(2\phi - \frac{\pi}{3}\right) \tag{7.7}$$

Comparison of Methods

It is interesting to compare the steady state torque speed curves for the three approximations. This is done in Fig 7.1,7.2, and 7.3. From the figures we see that Approximation A is not very accurate. We also see that Approximation B is quite accurate for $\phi = 30°$ and $\phi = 60°$. Approximation C is also excellent for $\phi = 30°$. Its accuracy as a function of ϕ is easily understood in terms of Fig. 6.8 - Fig. 6.11. The error of the approximations is quantified in Table 7.2. The value of error cited is found by summing the square of the error at a number of sample points, taking the square root, dividing by the number of points, and multiplying by one thousand. The points taken are regularly spaced and are over the range of ω_r such that the actual average torque is positive.

In order to obtain further verification of the results presented in this thesis, the Runga Kutta method of solving differential equations was used to generate a corresponding set of torque speed curves. The results are not shown here because the torque speed curves generated by the Runga Kutta

method are not distinguishable from those obtained from the analytical/numerical method presented in chapter five.

Table 7.2 Comparison of Approximations

	$\phi = 0°$	$\phi = 30°$	$\phi = 60°$
Approximation A	54.1	24.2	21.2
Approximation B	65.0	9.6	4.0
Approximation C	8.7	3.2	11.7

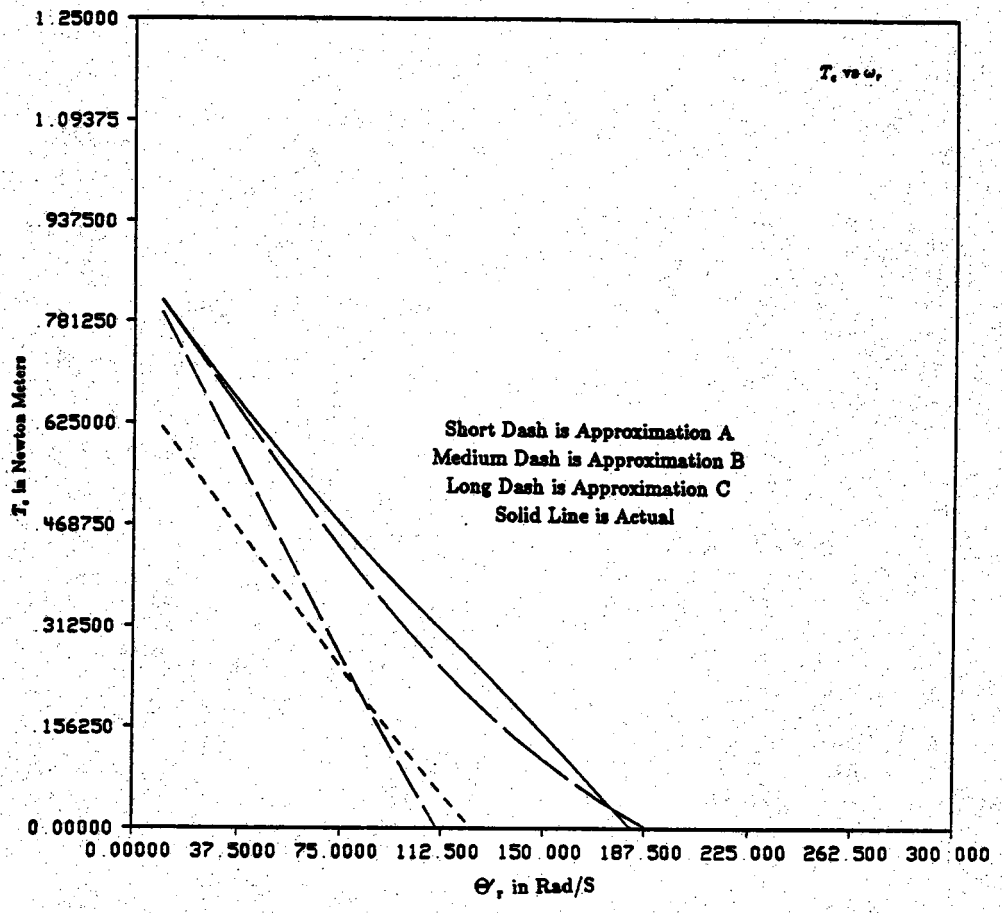

Figure 7.1 Torque Comparison for $\phi = 0^{\circ}$

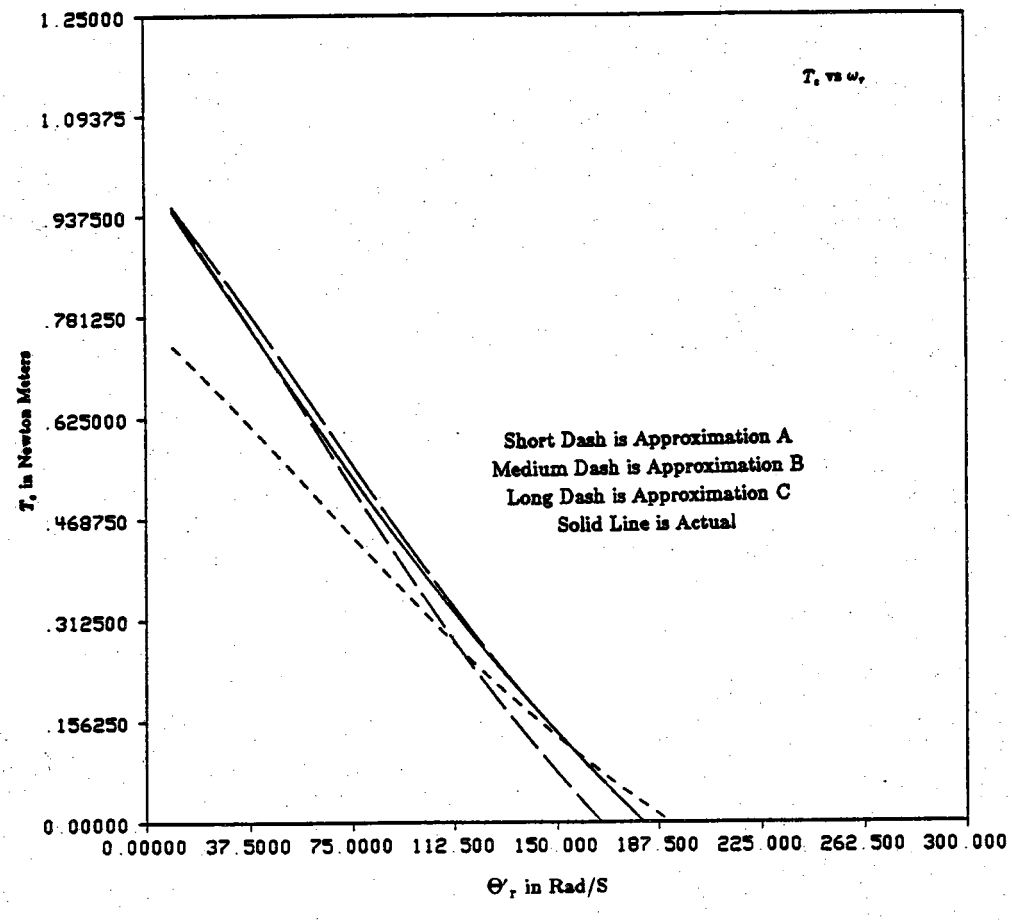

Figure 7.2 Torque Comparison for $\phi = 30°$

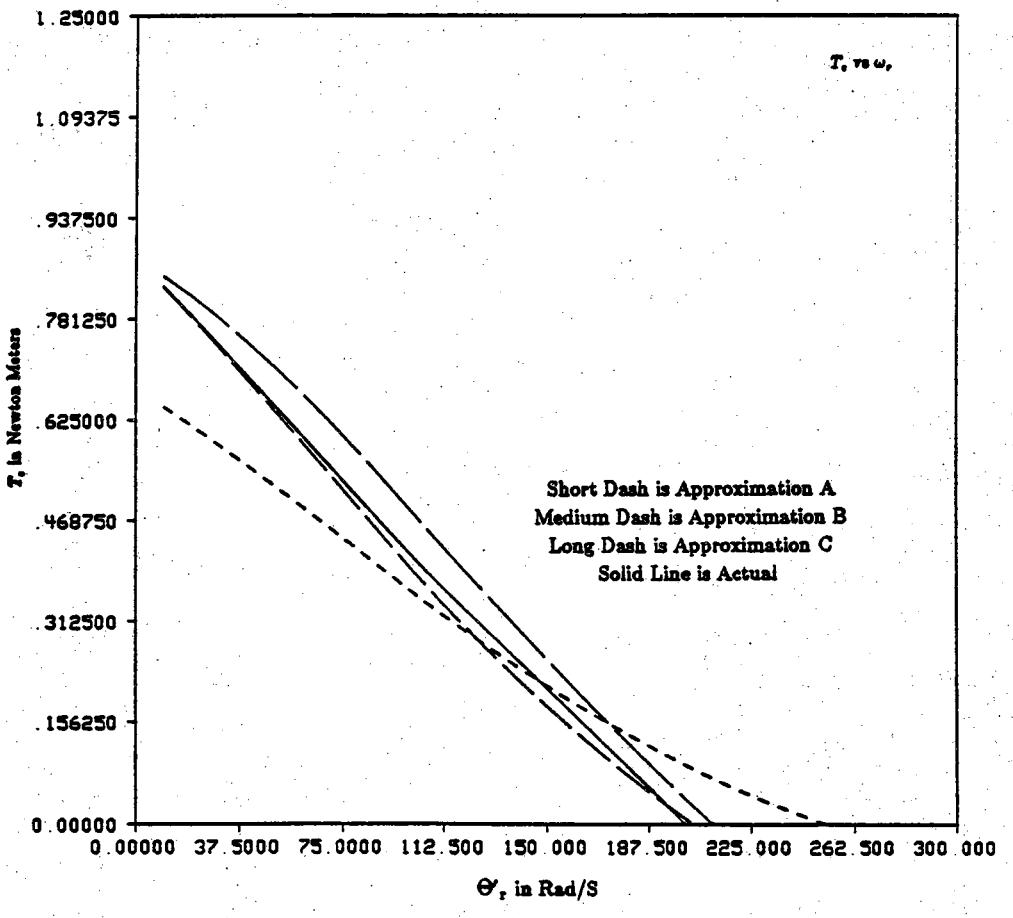

Figure 7.3 Torque Comparison for $\phi = 60°$

CHAPTER 8
CONCLUSION

The primary thrust of this thesis was to establish an efficient method of simulating the performance of the brushless dc motor 120° inverter system. The computational method presented is much faster than strictly numerical methods since numerical integration is avoided. In developing the computational method, various phenomenon associated with inverter operation such as N,P, and Z intervals, Z-N and Z-P transitions, and Z-N and Z-P domains were investigated. In particular, the location of the Z-N and Z-P domains within BSI II have been shown to have a profound influence on inverter operation. Also, inverter operation can be classified into distinct modes. This is useful in describing the operation of this system. Finally, it was demonstrated that the theory set forth can lead to analytical approximations for the torque speed characteristics. In particular, for the normal case where $\phi = 30°$, Approximation 3 was shown to be excellent.

LIST OF REFERENCES

[1] Nucera, Roberto R.,"Computation of Steady State Performance of an Electronically Commutated Motor," Master's Thesis, Purdue University, 1985.

[2] Risden, Melissa R., "Computation of the Steady State Performance of an Electronically Commutated Motor in the 120° Mode of Operation," Master's Thesis, Purdue University, 1986.

[3] Nucera, R. R., Sudhoff, S. D., Krause, P. C., "Computation of Steady State Performance of an Electronically Commutated Motor," accepted for IEEE Transactions.

[4] Iizuka, K., Uzuhashi, H., Kano, M., Endo T., Mohri, K., "Microcomputer Control for Sensorless Brushless Motor," IEEE Trans. on Industry Applications, Vol. IA-21, No. 4, pp. 595-601, May/June 1985.

[5] Krause, Paul C., *Analysis of Electric Machinery.* McGraw Hill, 1986.

[6] Krause, Paul C., Wasynczuk, Oleg., *Electromechanical Motion Devices.* Purdue University, 1987.

[7] Krause, Paul C., Wasynczuk, Oleg., *Inverter Systems Class Notes For EE495Y.* Purdue University, 1988.

APPENDIX

APPENDIX
MACHINE PARAMETERS

Every simulation result presented in this thesis is based on the same set of machine and inverter parameters. The value of all parameters necessary to typify the system is given in the following table.

Table A.1 - Machine Parameters

Parameter	Symbol	Value	Units
Inverter Input Voltage	V_{dc}	25	V
Flux Linkage Coefficient	λ'_m	83	mVS
Stator Inductance	L_s	12.1	mH
Stator Resistance	r_s	3.4	Ω
Number of Poles	P	4	none